An Analysis of the VLASS Proposal

Jim Condon[1]

National Radio Astronomy Observatory,
520 Edgemont Road, Charlottesville, VA 22903, USA

jcondon@nrao.edu

ABSTRACT

"The Jansky–Very Large Array Sky Survey (VLASS)" (SSG 2015) comprises two distinct S-band ($2 < \nu < 4$ GHz) surveys:
(1) The shallow (rms noise $\sigma_{\rm n} \approx 69$ μJy beam^{-1} ≈ 1.5 K at $\theta \approx 2\farcs5$ resolution) but wide (covering all $33,885$ deg^2 north of $\delta = -40°$) "All-sky" and
(2) the sensitive ($\sigma_{\rm n} \approx 1.5$ μJy beam^{-1} ≈ 0.32 K at $0\farcs8$ resolution or ≈ 0.13 K at $2\farcs0 \times 0\farcs8$ resolution) but narrow (10 deg^2 in three patches) "Deep."

All-Sky is intended to be a community resource, the JVLA update of the high-impact FIRST and NVSS VLA surveys made at 1.4 GHz. FIRST and NVSS succeeded for two reasons: (1) they are $> 10\times$ better in number of sources detected, sensitivity, resolution, position accuracy, etc. than prior "all-sky" radio surveys, and (2) they have not been surpassed for almost two decades, so their high citation rates have not diminished.

In contrast, (1) the proposed All-Sky is only about $1.5\times$ more sensitive than FIRST for point-source populations whose effective spectral index is $\langle\alpha\rangle \approx -0.7$, and its sensitivity to extended sources (e.g., many radio galaxies and quasars, diffuse sources in galaxy clusters, low-redshift star-forming galaxies) is about $3\times$ worse than FIRST and about $60\times$ worse than NVSS because its angular resolution is so high. The rms noise $\sigma_{\rm n}$ on survey images has units of apparent brightness (μJy beam^{-1} or K), not flux density (μJy), so the high-resolution All-Sky images will miss $> 25\%$ of all sources with flux densities $S > 5\sigma_{\rm n} \approx 350\,\mu$Jy, including entire low-brightness populations such as normal spiral galaxies, whose median S-band surface brightness is only $\langle T_{\rm b}\rangle \approx 0.17$ K $\ll 5 \times 1.5$ K. (2) All-Sky will probably be surpassed before its earliest completion date (2023) by the contemporary ASKAP EMU survey (Norris et al. 2011) covering the whole sky

[1]The National Radio Astronomy Observatory is a facility of the National Science Foundation operated by Associated Universities, Inc.

south of $\delta = +30°$, and by the complementary Westerbork WODAN survey north of $\delta = +30°$. EMU intends to reach $\sigma_{\rm n} = 10$ μJy beam^{-1} ≈ 0.06 K at $\theta = 10''$ resolution at L band ($1.1 < \nu < 1.4$ GHz), which is equivalent to $\sigma_{\rm n} \approx 6$ μJy beam^{-1} ≈ 0.01 K at S band. EMU *will* detect spiral galaxies and generate complete samples of all sources $10\times$ below the All-Sky detection limit for point sources. Nearly all multi-wavelength astronomers asking the question "Are my favorite objects radio sources?" will get better answers from EMU than from All-Sky.

The uniquely high angular resolution of All-Sky, and hence its poor surface-brightness sensitivity, was forced by a straw-man optical identification method that fails to distinguish between extended radio sources (e.g., core plus lobes and jets) and radio source components (brightness peaks on images), so it tries to identify individual clearly resolved radio lobes with unrelated galaxies. The high resolution of All-Sky is not necessary for identification reliability (except for radio stars), and it is counterproductive because it lowers identification completeness—All-Sky will miss $> 25\%$ of all sources with flux densities above its $5\sigma_{\rm n}$ detection limit. No radio detection, no optical identification. Incompleteness is actually worse than unreliability because incompleteness cannot be corrected, while sources with marginal identifications can be reobserved.

The high sensitivity and angular resolution of Deep is likely to remain unique until SKA Phase I is operating. Deep is qualitatively like the large PI VLA survey COSMOS, but bigger. Its top science goals are (1) a pilot survey for constraining dark energy by detecting the effect of weak gravitational lensing on distant radio sources and (2) studying the evolution of complete (flux-limited) galaxy samples. These goals conflict because resolving most faint sources for goal (1) implies sample incompleteness for goal (2). The proposal suggests that Deep will resolve most sources so it can detect weak lensing, but Deep won't resolve most sources so its completeness limit in μJy beam^{-1} can be conflated with source flux densities in μJy. The Deep proposal must fully address the angular-size distributions of μJy sources before it can be reviewed responsibly.

The VLASS will cost about 9,000 hours of JVLA observing time plus 20+ FTE-years of Socorro scientific staff effort for development. User feedback about the VLA time taken by FIRST and NVSS led to the Bridle et al. (1997) Report, which was ignored by the proposal but should be required reading. The front-loaded VLASS support requirements could divert most of the already-overloaded Socorro scientific staff from JVLA commissioning and helping observers for the next few years.

1. Introduction

The VLASS proposal originated in the community suggestion "it was time to think about a follow-on from NVSS and FIRST" (SSG 2015) that would exploit the new capabilities of the JVLA. The VLASS originally had no specific science goals or technical specifications, so white papers were solicited and discussed at a workshop preceding the January 2014 AAS meeting and reported at
`https://science.nrao.edu/science/surveys/vlass`
See Appendix A "Motivation and Process" of SSG (2015) for a longer history. I was a member of the workshop SOC and presented the "Skeptic's View" at the workshop.

The VLASS Survey Science Group (SSG) of all interested parties (mostly non-NRAO) was formed after the workshop and spent the next year developing the final VLASS proposal. As the SSG "designated skeptic," NVSS PI, and an NRAO employee, I had potential conflicts of interest. To minimize them, I participated in the SSG meetings but did not try to influence the choice of science goals, except to calculate their technical implications. After each draft VLASS proposal appeared, I sent to the SSG my "VLASS Notes" analyzing its strengths, weaknesses, and possible fixes. The present "An Analysis of the VLASS Proposal" update those notes to address the "final" VLASS proposal (SSG 2015).

The VLASS is so different from earlier surveys that a careful and quantitative analysis is needed to show it can meet its many different and sometimes incompatible science goals. In particular, high angular resolution and high completeness of flux-limited source samples don't mix. Simple quantities such as survey frequency and source flux density have to be redefined for observations with large fractional bandwidths. Questions like "How does optical/IR identification completeness and reliability depend on survey sensitivity and angular resolution?" or "How accurate are in-band spectral indices?" need quantitative answers. Sections 2, 3, and 4 present the technical calculations. The capabilities of the VLASS are compared with the proposed science goals is Section 5. Section 6 reviews VLASS justifications based on technical performance and predicted science impact. For the technically inclined, the ongoing debate on the angular resolution that yields the best optical identifications is detailed in Appendix A.

2. VLASS Specifications

The "final" VLASS proposal (SSG 2015) describes an S-band survey with two Tiers (Tier 1 = All-Sky and Tier 2 = Deep) that will use ~ 9000 hours of JVLA observing time in the B and A configurations. The VLA exposure calculator (for pointed observations

with 1.5 GHz input bandwidth, no frequency weighting, and "robust" (u, v) weighting) gave the Tier specifications at $\nu = 3$ GHz listed in the first two rows of Table 1 and plotted in Figure 1. The first six columns match Table 1 in SSG (2015), and the final two columns list their noise levels in brightness units. (Caveat: most of the Deep observing time is spent in the ECDFS field at declination $\delta \approx -28°$, where the 3 GHz beam is a $2\farcs0 \times 0\farcs8$ ellipse.) The last two rows are more accurate for surveys like the VLASS in which the integration time per position is proportional to primary beam solid angle, or ν^{-2} (Section 4.1.1). Thus the effective frequency of the VLASS is about 10% lower, the synthesized beamwidth is about 10% larger, and the rms noise is slightly lower than specified in SSG (2015).

The Executive Summary of the SSG (2015) stresses (original emphases) "Both components make optimal utilization of the Jansky VLA's unique capabilities: *high resolution imaging* and *exquisite point-source sensitivity*, critical for source identification; *wide bandwidth coverage*, enabling instantaneous spectral index determination; and *full polarimetry* with good performance even in lines of sight with high Faraday depth, enabling instantaneous rotation measure and Faraday structure determinations."

The uniquely *high angular resolution* chosen for the All-Sky is not critical for source identification reliability (Appendix A), and it comes at the cost of low completeness for flux-limited source samples, and hence low identification completeness. The high rms *surface brightness* noise levels (columns 7 and 8 in Table 1) of both VLASS Tiers mean that neither can detect low-brightness sources, normal star-forming galaxies in particular, no matter how high their total flux densities.

The *exquisite point-source sensitivity* at 3 GHz of All-Sky is only 1.5× better than FIRST for sources with mean spectral index $\langle\alpha\rangle \equiv d \ln S / d \ln \nu = -0.7$ and is 10× worse than the sensitivity of the planned EMU (Norris et al. 2011) survey (Table 2). The point-source sensitivity of Deep is unique and should remain so until SKA Phase I exists.

Table 1. VLASS Specifications

Tier	Component Name	Area (deg^2)	ν (GHz)	θ (arcsec)	$\sigma_{\rm n}$ (μJy/$\Omega_{\rm b}$)	$\sigma_{\rm n}$ (MJy sr^{-1})	$\sigma_{\rm n}$ (K)
1	All-Sky	33,885	3.000	2.5	69	0.42	1.51
2	Deep	10	3.000	0.8	1.5	0.088	0.32
1	All-Sky	33,885	2.682	2.8	65	0.31	1.42
2	Deep	10	2.682	0.9	1.5	0.069	0.32

The *wide bandwidth coverage* (2 to 4 GHz) enables instantaneous spectral-index determination in principle, but in practice it is useful only for very strong, compact sources because (1) the in-band α is so vulnerable to noise errors that a signal-to-noise ratio SNR ≈ 50 is required to reach $\sigma_\alpha \approx 0.1$, and (2) the spectral indices of extended sources are biased steep because the synthesized beam solid angle falls by 4× across the band (Section 4.2).

The relatively high VLASS center frequency (about twice the 1.4 GHz of most competing surveys) allows for higher angular resolution, reduces Faraday depolarization, and helps to protect the All-Sky snapshot images from being dynamic-range limited. The tradeoffs are (1) a smaller instantaneous field-of-view for discovering transients having durations shorter than the ~ 32 month cadence of All-Sky, (2) a lower instrumental survey speed (Section 4.1.3), and (3) a lower point-source detection rate for most radio sources (Section 4.1.4). If surveys at frequencies ν_1 and ν_2 detect the same numbers per steradian of radio sources stronger than S_1 and S_2, then the effective spectral index of the radio-source population can be defined as

$$\langle\alpha\rangle \equiv \ln(S_1/S_2)/\ln(\nu_1/\nu_2) \quad (1)$$

Over a wide range of frequencies near $\nu \sim 3$ GHz, $\langle\alpha\rangle = -0.7$ (Condon 1984) so, on average, sources are 1.58× weaker at 2.682 GHz than at 1.4 GHz. The $\sigma_n = 65\,\mu$Jy beam^{-1} 2.682 GHz VLASS All-Sky survey should detect about as many point sources per square degree as a $\sigma \approx 102\,\mu$Jy beam^{-1} 1.4 GHz survey. Table 2 can be used with Table 1 to compare the point-source and brightness sensitivities of VLASS with FIRST (Becker et al. 1995), NVSS (Condon et al. 1998), and EMU (Norris et al. 2011).

The main difficulty faced by any blind JVLA sky survey (as apposed to a survey directed at a list of known targets such as nearby stars) is that *the JVLA was not optimized for sky surveys*: (1) Its Field-of-View (FoV) is limited by the small primary beam of the large ($D = 25$ m) dishes, and each dish has only one primary beam. (2) The JVLA performance improvement over the original VLA is greatest at high frequencies, where the wider

Table 2. FIRST, NVSS, and EMU Specifications at 1.4 GHz and converted to 2.682 GHz using the mean source spectral index $\langle\alpha\rangle = -0.7$.

	Area	θ	σ_n (1.4 GHz)			σ_n (2.682 GHz, $\alpha = -0.7$)		
Name	(deg^2)	(arcsec)	(μJy/Ω_b)	(MJy sr^{-1})	(K)	(μJy/Ω_b)	(MJy sr^{-1})	(K)
FIRST	$\sim 10^4$	5.4	150	0.193	3.21	95	0.122	0.56
NVSS	3.4×10^4	45	450	0.0083	0.139	285	0.0053	0.024
EMU	3.1×10^4	10	10	0.0038	0.062	6.3	0.0024	0.011

bandwidths and new receivers multiply the sensitivities of targeted observations by an order of magnitude. However, FoVs and most source flux densities are lower at high frequencies, so sky-survey performance is only slightly better.

3. Flux Density, Peak Flux Density, and Brightness

The VLASS proposal (SSG 2015) lists the VLASS rms noise levels $\sigma_{\rm n}$ and source detection limits ($5\sigma_{\rm n}$) only in terms of "peak" flux densities $S_{\rm p}$ that are defined as flux density per beam (μJy beam^{-1}). "Beam" is shorthand for the restoring beam solid angle, which is

$$\Omega_{\rm b} = \frac{\pi\theta^2}{4\ln 2} \tag{2}$$

for a Gaussian restoring beam with half-power diameter θ.

Peak flux densities ($S_{\rm p}$) are not flux densities (S). Flux densities are properties of *astronomical sources* but not images, while peak flux densities depend on image resolution. Astrophysically useful source samples (e.g., samples used to construct luminosity functions and track galaxy evolution) should be complete above well-defined flux-density limits and not seriously biased against resolved sources whose peak flux densities are significantly lower than their flux densities. Peak flux densities are numerically equal to flux densities only for sources having angular diameters $\phi \ll \theta$. *Incompleteness for extended sources is the biggest weakness of the high-resolution VLASS.*

Conflating $S_{\rm p}$ and S systematically overestimates what a high-resolution survey can do. For example, "...the star-forming galaxy population becomes detectable at flux densities around $S_{1.4\ {\rm GHz}} \sim 1$ mJy beam^{-1}..." on page 8 of SSG (2015) should really be "...the star-forming galaxy population becomes detectable at flux densities around $S_{1.4\ {\rm GHz}} \sim 1$ mJy..." Although All-Sky can easily detect $S_{\rm p} \sim 1$ mJy beam^{-1} sources, most star-forming galaxies with $S_{1.4\ {\rm GHz}} \geq 1$ mJy fall below its $S_{\rm p} = 5\sigma_{\rm n} \approx 0.35$ mJy beam^{-1} detection limit. Another example is Figure 2 in SSG (2015), which shows the predicted Poisson counting errors in 3 GHz luminosity functions of star-forming galaxies at $z \sim 1$ and $z \sim 3$ that could be derived from surveys covering 2, 4, and 10 deg^2 to a depth of $S = 7.5\,\mu$Jy, in order to justify the Deep survey tier. However, the Deep detection limit is not $S = 7.5\,\mu$Jy; it is $S_{\rm p} = 7.5\,\mu$Jy beam^{-1} in a $\theta \approx 0\farcs8$ FWHM beam. If these faint sources are resolved enough to measure weak-lensing shear (Section 5.2), their peak flux densities S_p must be significantly lower than their total flux densities S and many sources with $S \geq 7.5\,\mu$Jy will not be detected. *A single survey can either detect most sources stronger than a certain flux density or it can resolve most sources, but it cannot do both.*

Peak flux densities are not really brightnesses either, even though they have the same *dimensions* as brightness. Brightnesses are conserved properties of *sources alone* and are independent of image resolution. Examples of proper brightness units are the MJy sr^{-1} preferred by infrared astronomers and the K (Kelvins) of Rayleigh-Jeans brightness temperature frequently used by radio astronomers. The apparent Rayleigh-Jeans brightness temperature in an image pixel with peak flux density S_p is

$$T_b = \frac{2\ln(2)c^2 S_p}{\pi k \theta^2 \nu^2} \ , \tag{3}$$

where $c \approx 3.00 \times 10^8$ m s^{-1} and $k \approx 1.38 \times 10^{-23}$ J K^{-1}. In Table 1 the rms noises in K (Column 8) were calculated from Equation 3. See Table 2 to compare them with the noise parameters of the 1.4 GHz FIRST (Becker et al. 1995), NVSS (Condon et al. 1998), and EMU (Norris et al. 2011) surveys.

Two surveys having the same sensitivity in μJy $beam^{-1}$ but different beam solid angles Ω_b will have different brightness sensitivities in K. For example, the $5\sigma_n$ detection limits of FIRST ($\theta = 5\farcs4$) and NVSS ($\theta = 45''$) are 1 mJy $beam^{-1}$ and 2.3 mJy $beam^{-1}$ respectively, so FIRST is more than twice as sensitive as the NVSS to sources with $\phi \ll 5\farcs4$ (Table 2). In terms of brightness, their rms image noises are $\sigma_n = 3.21$ K and 0.14 K respectively, so the NVSS is ~ 20 times as sensitive as FIRST to very extended sources ($\phi \gg 45''$). Equations 27 and 28 in Section 4.1.5 imply that FIRST and NVSS sensitivities are comparable for circular Gaussian sources of angular diameter $\phi \sim 6''$ (e.g., radio emission powered by star formation in a face-on disk galaxy) or narrow linear sources of length $\phi \sim 12''$ (e.g., radio jets powered by an AGN). Both VLASS tiers have higher angular resolutions and consequently lower brightness sensitivities.

If the brightness detection limit of a survey image is greater than the brightness of a source, that source will not be detected no matter how close it is, because source brightness is distance-independent. Most extragalactic sources have spectral indices α close ($\sigma_\alpha \sim 0.13$) to $\langle\alpha\rangle = -0.7$ (Condon 1984), so their Rayleigh-Jeans brightness temperatures vary with frequency as $T_b \propto \nu^{-2.7}$. The brightness temperature most relevant to sensitive extragalactic radio surveys is the median brightness temperature of radio sources powered by star formation in normal face-on spiral galaxies. It is $\langle T_b \rangle \sim 1$ K at 1.4 GHz (Hummel 1981), and at nearby frequencies it is

$$\frac{\langle T_b \rangle}{\mathrm{K}} \approx 2.5 \left(\frac{\nu}{\mathrm{GHz}} \right)^{-2.7} \ . \tag{4}$$

Surveys must have brightness sensitivity limits $5\sigma_n < \langle T_b \rangle$ to detect astrophysically complete samples of normal star-forming galaxies and measure their flux densities accurately. Thus the 1.4 GHz NVSS ($5\sigma_n \approx 0.7$ K) can detect and measure the flux densities of most nearby

spiral galaxies (Condon et al. 2002) but FIRST ($5\sigma_\mathrm{n} \approx 16$ K) cannot. The median $\nu = 2.682$ GHz brightness temperature of nearby spiral galaxies is $\langle T_\mathrm{b} \rangle \sim 0.17$ K. The $5\sigma_\mathrm{n} < \langle T_\mathrm{b} \rangle$ requirement means that 2.682 GHz VLASS images must have $\sigma_\mathrm{n} < 0.035$ K to detect most low-redshift spiral galaxies. Both VLASS tiers miss this requirement by an order of magnitude (Table 1), preventing VLASS images from tracing the star-formation history of the universe (Section 4.1.5).

For a survey to detect most radio sources powered by star formation, its beamwidth must satisfy

$$\left(\frac{\theta}{\mathrm{arcsec}}\right)^2 \geq 2.44 \left(\frac{\sigma_\mathrm{n}}{\mu\mathrm{Jy\ beam}^{-1}}\right)\left(\frac{\nu}{\mathrm{GHz}}\right)^{+0.7} . \quad (5)$$

At the point-source sensitivities of the VLASS tiers (Table 1), these minimum beamwidths are $\theta = 18''$ (All-Sky) and $2\farcs7$ (Deep). A JVLA survey that could detect most star-forming galaxies might use the C configuration at L band to replace All-Sky, but it would just be an inferior version of EMU ($\theta = 10''$, $\sigma_\mathrm{n} = 10\,\mu$Jy beam^{-1}, $\nu = 1.4$ GHz). Deep would better probe the cosmic evolution of star formation if it were done with the B configuration at either S band or L band. Neither tier of the proposed VLASS can detect a complete sample of nearby (e.g., $z < 0.5$) spiral galaxies and measure the flux densities needed to calculate their luminosity functions.

Columns 6–9 of Table 2 list the FIRST, NVSS, and EMU survey parameters converted to their 2.682 GHz equivalents for sources with flux-density spectral index $\alpha = -0.7$ (temperature spectral index -2.7) for direct comparison with the 2.682 GHz VLASS parameters in Table 1. The equivalent rms noise of the 1.4 GHz FIRST survey at 2.682 GHz is $\sigma_\mathrm{n} = 150\,\mu$Jy beam^{-1} $\times\ (2.682/1.4)^{-0.7} = 95\,\mu$Jy beam^{-1} so All-Sky ($\sigma_\mathrm{n} = 65\,\mu$Jy beam^{-1}) is only $1.5\times$ as sensitive for point sources. EMU ($\sigma_\mathrm{n} = 5.9\,\mu$Jy beam^{-1} at 2.682 GHz) is an order-of-magnitude more sensitive to point sources than any other "all sky" survey. For extended sources with $\phi \gg 5\farcs4$, FIRST has 2.682 GHz brightness noise $\sigma_\mathrm{n} = 3.21$ K $\times\ (2.682/1.4)^{-2.7} = 0.56$ K rms, which is $2.5\times$ as sensitive as All-Sky. Both EMU ($\sigma_\mathrm{n} = 11$ mK) and NVSS (24 mK) have much lower 2.682 GHz brightness noise levels.

Such tradeoffs involving point-source sensitivity, angular resolution, and sensitivity to extended sources are illustrated by the Hodge et al. (2011) 1.4 GHz Stripe 82 survey. It has rms noise $\sigma_\mathrm{n} = 52\,\mu$Jy beam^{-1} (equivalent to $\sigma_\mathrm{n} \approx 33\,\mu$Jy beam^{-1} at 2.682 GHz for $\alpha = -0.7$) and $\theta \gtrsim 1\farcs8$, which is $3\times$ the point-source sensitivity, $3\times$ the angular resolution, and $3^{-1}\times$ the brightness sensitivity of FIRST. The Stripe 82 survey failed to detect 22% of the FIRST sources with $S \geq 1000\,\mu$Jy, although some of the missing FIRST "sources" may only be FIRST sidelobes of stronger sources. Comparison with the far more sensitive COSMOS survey (Bondi et al. 2008) indicates the Stripe 82 source-detection completeness

is $\lesssim 0.5$ for $S \leq 500\,\mu$Jy.

Figure 1 and Table 2 of SSG (2015) use the Wilman et al. (2008) SKADS sky simulation to predict the sky densities of extragalactic sources that should be detected by All-Sky and Deep. That figure shows a total of ≈ 380 sources deg^{-2} stronger than $S = 350\,\mu$Jy at 3 GHz, but only 290 sources deg^{-2} brighter than the All-Sky detection limit $S_{\rm p} = 350\,\mu$Jy beam^{-1} = $46\,\mu$Jy arcsec^2, for a *cumulative* completeness of only 75%. That is, All-Sky is predicted to miss about 25% of *all* sources stronger than $S = 350\,\mu$Jy. Even the predicted All-Sky detection rate of 290 sources deg^{-1} seems optimistic, given that FIRST detected only ≈ 90 sources deg^{-2}. Table 2 of SSG (2015) indicates that All-Sky will detect about 10^7 sources. EMU (Norris et al. 2011) is expected to detect about 7×10^7 sources.

4. Survey Performance Metrics

The ubiquitous "survey speed" performance metric is useful only for comparing the rates at which different telescopes can cover the sky down to a specified point-source rms noise in μJy beam^{-1} at a given frequency. Section 4 defines the meaning(s) of "frequency" in targeted and survey observations made with large fractional bandwidths and introduces speed metrics for comparing targeted and sky-survey observations with a given array (Sections 4.1.1 and 4.1.2), metrics for comparing sky surveys made at different frequencies (Section 4.1.4), and metrics for comparing the rates that surveys can detect extended sources as well as point sources (Section 4.1.5). Section 4.2 covers "in band" spectral indices and their noise uncertainties.

4.1. Point Sources

4.1.1. Instrumental Sensitivity

The noise variance in an image made with "natural" weighting in the (u, v) plane is given by the simple radiometer equation for interferometers:

$$\sigma_{\rm n}^2 = \frac{S_{\rm sys}^2}{\eta_{\rm c}^2 n_{\rm p} N(N-1)\tau B}\ , \tag{6}$$

where $S_{\rm sys}$ is the "system equivalent flux density" (SEFD) of noise for each antenna, $\eta_{\rm c} \geq 0.8$ is the correlator efficiency, $n_{\rm p} = 2$ is the number of polarization channels contributing to the image, N is the number of working antennas in the array (the VLA exposure calculator assumes $N = 25$), τ is the integration time, and B is the instantaneous total bandwidth

(the VLA exposure calculator should be used with $B = 1.5$ GHz at S band to allow for RFI excision). Both $\sigma_{\rm n}$ and $S_{\rm sys}$ are really peak flux densities, not flux densities. The "robust" (u, v) weighting used in the VLA exposure calculator at `https://obs.vla.nrao.edu/ect/` multiplies the natural-weighting rms noise by ≈ 1.20.

Equation 6 is valid for images with small fractional bandwidths, but the VLA S band spans the octave frequency range $\nu_{\rm min} = 2$ GHz to $\nu_{\rm max} = 4$ GHz. Equation 6 also applies to the pointing centers of broadband images in which $S_{\rm sys}^2$ and τ are independent of frequency, as is often the case for targeted observations imaging sources much smaller than the primary beamwidth, and the spectral channels are unweighted (that is, channels with equal bandwidths have equal weights).

It appears that the variation of $S_{\rm sys}$ with frequency across the JVLA S band has not been measured accurately enough (Condon 2015, private communication), so all VLASS sensitivity calculations may have to be revised slightly. Such a measurement is easy to make, and it should be made before the VLASS external review. For now, I assume $S_{\rm sys}$ is nearly independent of frequency.

Source flux density is a narrowband quantity that can vary with frequency. What is the *apparent* flux density of a point source in an image made from data spanning a large fractional bandwidth? Most continuum radio sources have nearly power-law spectra $S(\nu)/S_0 = (\nu/\nu_0)^\alpha$, where ν_0 is any arbitrary reference frequency. The (spectrally) unweighted image flux density $S_{\rm u}$ of a point source is

$$S_{\rm u} = \frac{\int S(\nu) d\nu}{\int d\nu} \approx S_0 \nu_0^{-\alpha} \left(\frac{\nu^{\alpha+1}}{\alpha+1} \Big|_{\nu_{\rm min}}^{\nu_{\rm max}} \right) \Big/ (\nu_{\rm max} - \nu_{\rm min}) \ , \quad (\alpha \neq -1) \tag{7}$$

so

$$\frac{S_{\rm u}}{S_0} = \left(\frac{\nu_0^{-\alpha}}{\alpha+1} \right) \left(\frac{\nu_{\rm max}^{\alpha+1} - \nu_{\rm min}^{\alpha+1}}{\nu_{\rm max} - \nu_{\rm min}} \right), \quad (\alpha \neq -1) \tag{8}$$

For any spectral index α there is an "effective" frequency $\nu_{\rm u}$ at which the unweighted image flux density $S_{\rm u}$ equals the actual flux density of the source $S(\nu_{\rm u})$:

$$\frac{S_{\rm u}}{S(\nu_{\rm u})} = \left(\frac{\nu_{\rm u}^{-\alpha}}{\alpha+1} \right) \left(\frac{\nu_{\rm max}^{\alpha+1} - \nu_{\rm min}^{\alpha+1}}{\nu_{\rm max} - \nu_{\rm min}} \right) = 1 \ , \quad (\alpha \neq -1) \tag{9}$$

The effective frequency of an unweighted image for sources with spectral index α is

$$\nu_{\rm u} = \left[\left(\frac{1}{\alpha+1} \right) \left(\frac{\nu_{\rm max}^{\alpha+1} - \nu_{\rm min}^{\alpha+1}}{\nu_{\rm max} - \nu_{\rm min}} \right) \right]^{1/\alpha} \ , \quad (\alpha \neq -1) \tag{10}$$

Except for sources with strongly inverted spectra $\alpha \geq +1$, $\nu_{\rm u}$ is lower than the arithmetic mean frequency $\bar{\nu} = (\nu_{\rm max} + \nu_{\rm min})/2$ (= 3 GHz for the JVLA at S band) that has conventionally been called the observing frequency.

It is useful to choose a single effective image frequency that best characterizes the unweighted VLA S-band images for most sources. The natural choice is $\nu_{\rm u}(\langle\alpha\rangle)$, where $\langle\alpha\rangle = -0.7$; it is $\nu_{\rm u} \approx 2.903$ GHz. The ratio $S_{\rm u}/S(2.903\ {\rm GHz})$ of the unweighted image flux density to the true 2.903 GHz flux density varies slowly with source α as shown in the bottom panel of Figure 2. This ratio is in error by $< 1\%$ for all $-1.2 < \alpha < +0.5$, the spectral range encompassing nearly all sources in a flux-limited sample selected at frequencies near $\nu \sim 3$ GHz. Thus an unweighted VLA S-band image spanning $2 \leq \nu\,({\rm GHz}) \leq 4$ should yield accurate and meaningful 2.903 GHz flux densities for nearly all radio sources *close to the pointing center*.

However, for broadband mosaiced sky surveys like the VLASS, the integration time τ at each position varies with frequency as $\tau(\nu) \propto \nu^{-2}$ because the primary-beam solid angle is proportional to ν^{-2}. Minimum survey image noise is attained by weighting each spectral channel by the inverse of its noise variance, so the weight assigned to the ith spectral channel should be $W_{\rm i} \propto \tau(\nu_{\rm i}) \propto \nu_{\rm i}^{-2}$ if the channels all have the same bandwidth. Comparing the noise variance $\sigma_{\rm w}^2$ of a survey image based on weighted spectral channels spanning the frequency range from $\nu_{\rm min} = 2$ GHz to $\nu_{\rm max} = 4$ GHz with the VLASS sensitivity originally calculated from the unweighted Equation 6 at $\bar{\nu} = 3$ GHz for the VLASS gives

$$\frac{\sigma_{\rm w}^2}{\sigma_{\rm n}^2} = \frac{\int d\nu}{\int (\nu/\bar{\nu})^{-2} d\nu} = \frac{\nu_{\rm min}\,\nu_{\rm max}}{\bar{\nu}^2} = \frac{8}{9} \tag{11}$$

Properly weighting the spectral channels by $(\nu/\bar{\nu})^{-2}$ lowers the originally calculated VLASS image noise by the factor $\sigma_{\rm w}/\sigma_{\rm n} \approx 0.943$.

Spectral weighting $W \propto \nu^{-2}$ also lowers the weighted arithmetic mean frequency $\bar{\nu}_{\rm w}$ to

$$\bar{\nu}_{\rm w} = \frac{\int (\nu/\bar{\nu})^{-2} \nu\, d\nu}{\int (\nu/\bar{\nu})^{-2}\, d\nu} = \frac{\int \nu^{-1} d\nu}{\int \nu^{-2} d\nu} = \left(\frac{\nu_{\rm min}\,\nu_{\rm max}}{\nu_{\rm max} - \nu_{\rm min}}\right) \ln\!\left(\frac{\nu_{\rm max}}{\nu_{\rm min}}\right) . \tag{12}$$

In the case of the VLASS,

$$\bar{\nu}_{\rm w} = \left(\frac{2 \cdot 4}{4 - 2}\right) \ln\!\left(\frac{4}{2}\right)\ {\rm GHz} = 4 \ln 2\ {\rm GHz} \approx 2.773\ {\rm GHz} \tag{13}$$

Note that this weighted frequency is a property of the instrument and survey frequency range only; it is independent of radio source spectra.

If a point source has flux density $S(\nu)/S_0 = (\nu/\nu_0)^{\alpha}$, its apparent flux density in a weighted broadband survey image is

$$S_{\rm w} = \frac{\int (\nu/\nu_0)^{-2} S(\nu) d\nu}{\int ((\nu/\nu_0)^{-2} d\nu} = S_0 \nu_0^{-\alpha} \left(\frac{\nu^{\alpha-1}}{\alpha - 1}\bigg|_{\nu_{\rm min}}^{\nu_{\rm max}}\right) \Big/ \left(-\nu^{-1}\right)\Big|_{\nu_{\rm min}}^{\nu_{\rm max}}, \quad (\alpha \neq -1) \tag{14}$$

$$\frac{S_{\rm w}}{S_0} = \left(\frac{\nu_0^{-\alpha}}{1-\alpha}\right)\left(\frac{\nu_{\rm max}^{\alpha-1} - \nu_{\rm min}^{\alpha-1}}{\nu_{\rm max}^{-1} - \nu_{\rm min}^{-1}}\right) , \quad (\alpha \neq -1) \tag{15}$$

The frequency $\nu_{\rm w}$ at which the weighted image flux density is equals the actual source flux density satisfies

$$\frac{S_{\rm w}}{S(\nu_{\rm w})} = \left(\frac{\nu_{\rm w}^{-\alpha}}{1-\alpha}\right)\left(\frac{\nu_{\rm max}^{\alpha-1} - \nu_{\rm min}^{\alpha-1}}{\nu_{\rm max}^{-1} - \nu_{\rm min}^{-1}}\right) = 1 , \quad (\alpha \neq -1) . \tag{16}$$

It is

$$\nu_{\rm w} = \left[\left(\frac{1}{1-\alpha}\right)\left(\frac{\nu_{\rm max}^{\alpha-1} - \nu_{\rm min}^{\alpha-1}}{\nu_{\rm max}^{-1} - \nu_{\rm min}^{-1}}\right)\right]^{1/\alpha} , \quad (\alpha \neq -1) \tag{17}$$

The top panel of Figure 3 shows $\nu_{\rm w}(\alpha)$ for the VLASS.

The single effective frequency that best characterizes spectrally weighted survey images for most sources is $\nu_{\rm w}(\langle\alpha\rangle)$, where $\langle\alpha\rangle = -0.7$; it is $\nu_{\rm w} \approx 2.682$ GHz for the VLASS. Then $S_{\rm w}/S(2.682\ {\rm GHz})$ varies slowly with α as shown in the bottom panel of Figure 3. This ratio is in error by $< 1\%$ for all $-1.2 < \alpha < +0.5$, the spectral range encompassing nearly all sources in a flux-limited sample at frequencies near $\nu \sim 3$ GHz. Equation 17 demonstrates that the broadband VLASS images should yield accurate and meaningful 2.682 GHz flux densities for nearly all point sources.

In summary, the original unweighted VLASS with nominal $\bar{\nu} = 3$ GHz is really a frequency-weighted survey with effective frequency $\nu_{\rm e} \approx 2.682$ GHz and about 6% lower rms noise. At 2.682 GHz the typical source with $\alpha = \langle\alpha\rangle = -0.7$ is $(2.682/3)^{\langle\alpha\rangle} \approx 1.082$ times stronger than it is at 3 GHz, so the frequency-weighted VLASS images should reveal about as many point sources per steradian as a 3 GHz unweighted survey in about 76% of the originally proposed observing time.

For the revised All-Sky survey with three scans and robust (u, v) weighting, the VLA exposure calculator predicts an rms noise $\sigma_{\rm n} \approx 69$ μJy beam^{-1} at $\bar{\nu} = 3$ GHz appropriate for unweighted targeted observations. With optimum survey frequency weighting, the rms noise drops to $\sigma_{\rm w} \approx 65$ μJy beam^{-1}, the effective frequency becomes $\nu_{\rm w} = 2.682$ GHz, and the source detection rate should match that of an unweighted 3 GHz survey with rms noise $\sigma_{\rm n} \approx 60$ μJy beam^{-1}.

4.1.2. Instrumental Speed for Directed Observations

The integration time τ required to reach a given noise $\sigma_{\rm n}$ in a single pointing can be obtained from the radiometer Equation 6; it is

$$\tau = \frac{1}{\sigma_{\rm n}^2}\left[\frac{S_{\rm sys}^2}{\eta_{\rm c}^2 n_{\rm p} N(N-1)}\right]\frac{1}{B} \tag{18}$$

so the *instrumental* speed $\dot{n}$ for directed observations defined by

$$\dot{n} \equiv \frac{1}{\tau} = \sigma_{\rm n}^2\left[\frac{\eta_{\rm c}^2 n_{\rm p} N(N-1)}{S_{\rm sys}^2}\right]B \tag{19}$$

is a purely instrumental figure-of-merit equal to the rate at which directed observations of point sources can be made with rms noise $\sigma_{\rm n}$. At frequencies $\nu \lesssim 10$ GHz the quantity in brackets is nearly the same for both the old VLA and the new JVLA, but the JVLA's usable bandwidth (ranging from $B \sim 600$ MHz at 1.5 GHz to $B \sim 8$ GHz above 18 GHz) is one or two orders of magnitude larger than the correlator-limited bandwidth of the old VLA, which was 50 or 100 MHz depending on the array configuration, field size, and the tolerable amount of bandwidth smearing. Thus *the JVLA is faster than the old VLA by one to two orders of magnitude for a typical user program* making a directed observation or a directed survey targeting a sample of n discrete sources.

4.1.3. Instrumental Survey Speed

For a continuum sky survey covering a much larger solid angle than a single field-of-view $\Omega_{\rm FoV}$, the figure-of-merit corresponding to $\dot{n}$ in Equation 19 is the *instrumental survey speed* $\dot{\Omega}$ defined by

$$\dot{\Omega} \equiv \frac{\Omega_{\rm FoV}}{\tau} = \dot{n}\Omega_{\rm FoV} \tag{20}$$

Instrumental survey speed measures the rate of sky coverage for a given rms noise $\sigma_{\rm n}$, and it is usually expressed in units of deg^2 hour^{-1}. Note that this traditional definition of survey speed does not include channel weighting (Section 4.1), so it slightly underestimates the potential speed of surveys with large fractional bandwidths.

Primary beams are approximately Gaussian, so the primary beam solid angle is

$$\Omega_{\rm pb} \approx \frac{\pi\theta_{\rm pb}^2}{4\ln 2} \approx 1.13\theta_{\rm pb}^2 \ , \tag{21}$$

where

$$\theta_{\rm pb} \approx \left(\frac{1.09\lambda}{D}\right) \text{ rad} \approx 0.75\left(\frac{\nu}{\rm GHz}\right)^{-1} \text{ deg} \tag{22}$$

is the FWHM primary beamwidth of the VLA's $D = 25$ m antennas. For sensitivity calculations, the effective field-of-view of a single Gaussian primary beam is exactly half the primary beam solid angle (Condon et al. 1998):

$$\Omega_{\rm FoV} = \frac{\Omega_{\rm pb}}{2} \approx 0.32 \left(\frac{\nu}{\rm GHz} \right)^{-2} \ {\rm deg}^{-2} \ . \tag{23}$$

It turns out that the instrumental survey speeds of both the old VLA and the new JVLA are well approximated by the convenient expression

$$\left(\frac{\dot{\Omega}}{\rm deg^2 \ hr^{-1}} \right) \approx \left(\frac{\sigma_{\rm n}}{\mu{\rm Jy \ beam^{-1}}} \right)^2 \left(\frac{S_{\rm sys}}{\rm Jy \ beam^{-1}} \right)^{-2} \left(\frac{B}{\rm MHz} \right) \left(\frac{\nu}{\rm GHz} \right)^{-2} \tag{24}$$

Because $\Omega_{\rm FoV}$ is proportional to ν^{-2}, Equations 20 and 24 imply that the speed of the JVLA (or any other radio telescope, even one with multiple beams like ASKAP) for surveys falls as ν^{-2} relative to the speed for directed observations. *This pushes large surveys to lower frequencies when competing for telescope time against targeted user proposals.*

4.1.4. Point-Source Survey Speed

Note that Equations 19 and 20 respectively defining the speeds for directed observations and for blind surveys describe purely *instrumental* properties; the spectra of actual radio sources were not considered. If the goal of a sky survey at frequency ν is to detect the largest number of point sources per steradian in a given observing time, source spectra must be taken into account. Nearly all discrete radio sources are extragalactic at mJy and μJy levels, with effective spectral index $\langle \alpha \rangle \approx -0.7$ (Condon 1984). Thus the rms image noise of a survey at frequency ν_1 should be multiplied by $(\nu_2/\nu_1)^{\langle \alpha \rangle}$ to compare with another survey at frequency ν_2.

This leads to the definition of the *point-source survey speed* $\dot{\Omega}_{\rm s}$ needed to compare the point-source detection rates of sky surveys made at two different frequencies ν_1 and ν_2:

$$\frac{\dot{\Omega}_{\rm s}(\nu_1)}{\dot{\Omega}_{\rm s}(\nu_2)} \equiv \frac{\dot{\Omega}(\nu_1)}{\dot{\Omega}(\nu_2)} \left(\frac{\nu_1}{\nu_2} \right)^{2\langle \alpha \rangle} \ . \tag{25}$$

Because $\dot{\Omega} \propto \nu^{-2}$ and $\langle \alpha \rangle = -0.7$, $\dot{\Omega}_{\rm s} \propto \nu^{-3.4}$ for fixed bandwidth B and $S_{\rm sys}$. If $B \propto \nu$, then $\dot{\Omega}_{\rm s} \propto \nu^{-2.4}$, which is still a steep frequency dependence strongly favoring surveys at lower frequencies. For the VLA and JVLA at frequencies 1 GHz $< \nu <$ 10 GHz,

$$\left(\frac{\dot{\Omega}_{\rm s}}{\rm deg^2 \ hr^{-1}} \right) \approx \left(\frac{\sigma_{\rm n}}{\mu{\rm Jy \ beam^{-1}}} \right)^{-2} \left(\frac{S_{\rm sys}}{\rm Jy} \right)^{-2} \left(\frac{B}{\rm MHz} \right) \left(\frac{\nu}{\rm GHz} \right)^{-2} \left(\frac{\nu}{\nu_0} \right)^{-1.4} \tag{26}$$

Column 5 of Table 3 shows the instrumental survey speeds $\dot{\Omega}$ at 1.5 GHz (L band), 3.0 GHz (S band), 6.0 GHz (C band), and 10.0 GHz (X band) for $\sigma_{\rm n} = 100\,\mu$Jy beam^{-1}. The L and S band instrumental survey speeds are nearly equal and much faster than the shorter-wavelength bands, but that doesn't mean that the L and S bands are nearly equal for detecting sources in sky surveys. Column 6 of Table 3 was calculated from Equation 25 using $\nu_0 = 1.5$ GHz for the fiducial frequency at which $\dot{\Omega} = \dot{\Omega}_{\rm s}$. The source survey speed $\dot{\Omega}_{\rm s}$ is highest at 1.5 GHz and falls rapidly at higher frequencies because the field-of-view is getting smaller and the sources are getting weaker.

The choice of S band instead of L band for the VLASS costs about a factor of 2.4 in observing time (e.g., 9000 hours versus 3800 hours needed to detect the same number of sources), so it needs to be justified in terms of dynamic-range limitations (a potential problem for "snapshot" surveys like FIRST, NVSS, and All-Sky), angular resolution, spectral-index information, Faraday rotation, cadence for transients, etc. It is not sufficient to dismiss L band on the grounds that the instrumental survey speed $\dot{\Omega}$ is about the same as at S band.

The original ($\sigma = 100\ \mu$Jy beam^{-1}) version of All-Sky can also be compared with 1.4 GHz VLA surveys such as FIRST (Becker et al. 1995). The VLA observational status summary for July 1996 gives $\sigma_{\rm n} = 60\,\mu$Jy beam^{-1} after $\tau = 10$ min for a naturally weighted 1.4 GHz image made with the nominal 100 MHz bandwidth. The nominal bandwidth of FIRST was $B \approx 50$ MHz so $\sigma_{\rm n} \approx 35\,\mu$Jy beam^{-1} after $\tau = 1$ hr. With $\Omega_{\rm FoV} \approx 0.163$ deg^2 at 1.4 GHz, the FIRST point-source survey speed relative to $\nu_0 = 1.5$ GHz is $\dot{\Omega}_{\rm s} \approx 1.5$ deg^2 hr^{-1}.

The (original) VLASS source survey speed is only a 4× improvement over FIRST, while regular users competing for the same JVLA time are getting a 10× to 100× speed improvement over the VLA on their directed observations, making it 2.5× to 25× harder to justify taking time from directed observations to make VLASS than it was to justify FIRST

Table 3. JVLA Instrumental and Point-Source Survey Speeds

ν (GHz)	$S_{\rm sys}$ (Jy beam)$^{-1}$	B (MHz)	$\Omega_{\rm FoV}$ (deg^2)	$\dot{\Omega}$ (deg^2/hr)	$\dot{\Omega}_{\rm s}$ (deg^2/hr)	VLASS/ FIRST
1.5	420	600	0.142	15.1	15.1	10
3.0	370	1500	0.035	16.5	6.3	4
6.0	310	3400	0.0089	7.2	1.0	0.7
10.0	250	3400	0.0032	3.0	0.21	0.14

and NVSS. *This factor should be considered in comparisons that use FIRST and NVSS to justify taking time from directed observations to make the VLASS (Section 6).*

Column 7 of Table 3 lists the JVLA/FIRST source survey speed ratios for point sources with $\langle\alpha\rangle = -0.7$. A JVLA point-source survey should be faster than the original FIRST by a factor of 10 at L band and by a factor of 4 at S band, but slower than FIRST at C band and X band. For surveys of $\langle\alpha\rangle = -0.7$ point-source populations, the JVLA at 3 GHz is only $\sim 4\times$ as fast or $\sim 2\times$ as sensitive as the VLA was at 1.4 GHz. That's why the originally proposed 3 GHz VLASS All-Sky survey exclusive of WIDE covered just over twice the FIRST survey area with slightly worse sensitivity to point sources, so it would have needed about half of the 4000 hours spent on FIRST. The originally proposed 3 GHz VLASS WIDE survey covered about the same solid angle as FIRST with $\sim 1.8\times$ better point-source sensitivity, so it would have needed about 3000 hours.

The revised VLASS survey speeds with survey-weighted frequency channels and natural (u, v) weighting would be about 32% higher, but the increased noise from robust (u, v) weighting actually slows down the revised VLASS survey speed by about 9%.

4.1.5. Extended-Source Sensitivity

The preceding parts of Section 4.1 apply only to sources much smaller than the survey point-spread function (PSF). The apparent brightness distribution of a source on an image is the convolution of the PSF and the actual source brightness distribution. Under convolution, the total flux density is conserved and the source area on the image is the sum of the PSF and source areas, so the peak flux density = flux/area on the image falls accordingly. For simplicity, consider a circular Gaussian source (e.g., the disk of a face-on star-forming galaxy) of angular diameter ϕ and total flux density S. Its peak flux density $S_{\rm p}$ in an image with a circular Gaussian PSF of FWHM diameter θ will be

$$\left(\frac{S_{\rm p}}{S}\right) = \left(\frac{\theta^2}{\phi^2 + \theta^2}\right) . \tag{27}$$

The analog of Equation 27 for a narrow linear source (e.g., a radio core plus twins jets and/or lobes powered by an AGN, or an edge-on thin disk) with an approximately Gaussian brightness profile is

$$\left(\frac{S_{\rm p}}{S}\right) = \left(\frac{\theta^2}{\phi^2 + \theta^2}\right)^{1/2} \tag{28}$$

For example, the Deep survey has $\theta = 0\farcs9$ resolution at 2.682 GHz and a detection limit $S_{\rm p} = 7.5\,\mu$Jy beam^{-1}. If a face-on star-forming galaxy at redshift $z = 0.2$ has a

FWHM diameter of 5 kpc, its angular size will be $\phi = 3\farcs1$. Deep can detect such a galaxy only if its flux density is greater than

$$S = S_{\rm p}\left(\frac{\phi^2+\theta^2}{\theta^2}\right) = 7.5\,\mu{\rm Jy\ beam}^{-1}\cdot\left(\frac{3.1^2+0.9^2}{0.9^2}\right){\rm beams} = 96\,\mu{\rm Jy} \qquad (29)$$

If the disk were edge-on, Deep could detect it only if $S \geq 27\,\mu$Jy.

In the limit of sources much larger than the beam ($\phi \gg \theta$), $S_{\rm p}/S \rightarrow (\theta/\phi)^2$ and it makes sense to describe sources in terms of their brightness temperatures

$$T_{\rm b}({\rm K}) = \frac{2\ln(2)c^2 S}{\pi k\phi^2\nu^2} \approx 1.22\left(\frac{S}{\mu{\rm Jy}}\right)\left(\frac{\phi}{\rm arcsec}\right)^{-2}\left(\frac{\nu}{\rm GHz}\right)^{-2}. \qquad (30)$$

The rms sensitivities in Kelvins of brightness temperature at 2.682 GHz are listed for both VLASS tiers and for comparable surveys in the rightmost columns of Tables 1 and 2, respectively.

4.2. Point-Source Spectral Indices

The JVLA's octave bandwidth is large enough to yield useful VLASS in-band spectral indices, at least for fairly strong point sources. Most radio sources have nearly power-law spectra, so their spectral indices $\alpha \equiv d\ln S/d\ln\nu$ can be derived from linear fits of many narrow-band channel flux densities to $\ln(S/S_0) = \alpha\ln(\nu/\nu_0)$, where S_0 is the flux density at some fiducial frequency ν_0. The accuracy with which the slope α of the linear fit can be determined from the noisy channel flux densities is proportional the length

$$l = \ln(\nu_{\rm max}) - \ln(\nu_{\rm min}) = \ln(\nu_{\rm max}/\nu_{\rm min}) \qquad (31)$$

of the bandwidth "lever arm" in ln(frequency) space. Ideally $l = \ln(4\ {\rm GHz}/2\ {\rm GHz}) \approx 0.693$ for the VLASS; in practice l may shrink if RFI preferentially eliminates channels near the ends of the frequency range.

Traditional two-point spectral indices α determined from two narrow-band flux densities S_1 and S_2 measured at frequencies ν_1 and ν_2 with rms noises σ_1 and σ_2 have rms noise errors

$$\sigma_\alpha = \frac{[(\sigma_1/S_1)^2 + (\sigma_2/S_2)^2]^{1/2}}{|\ln(\nu_1/\nu_2)|} \qquad (32)$$

For example, the $\nu_1 = 0.327$ GHz WENSS survey has $\sigma_1 \approx 3.6$ mJy and the $\nu_2 = 1.4$ GHz NVSS survey has $\sigma_2 \approx 0.45$ mJy for point sources. The rms width of the spectral-index distribution of "normal spectrum" sources in flux-limited samples is $\sigma_\alpha \approx 0.13$ (Condon

1984), so the measured spectral indices of sources with $\alpha \approx -0.7$ should have errors smaller than this to be useful. If we require $\sigma_\alpha \leq 0.1$ for a source with $\alpha = -0.7$, Equation 32 implies $S_2 > 9.5$ mJy at $\nu_2 = 1.4$ GHz or $S(2682\ \mathrm{GHz}) > 6.0$ mJy. Can All-Sky "in-band" or "instantaneous" spectra lower this sensitivity limit significantly?

The ideal (ignoring frequencies lost to RFI) VLASS All-Sky would span 2 to 4 GHz uniformly with a large number $N \gg 1$ of narrow frequency channels. For comparison with standard equations for linear least-squares fits (Bevington 1969), the power-law approximation

$$\ln(S) = \ln(S_0) + \alpha \ln(\nu/\nu_0) \ , \tag{33}$$

can be written as

$$y = a + bx \ , \tag{34}$$

where

$$y = \ln(S), \quad a = \ln(S_0), \quad b = \alpha, \quad \text{and} \quad x = \ln(\nu/\nu_0) \ . \tag{35}$$

In the ith frequency channel, $x_\mathrm{i} = \ln(\nu_\mathrm{i}/\nu_0)$, $y_\mathrm{i} = \ln(S_\mathrm{i})$ is the measured flux density, and σ_i is the rms uncertainty in $y_\mathrm{i} = \ln(S_\mathrm{i})$. Because $d\ln(S_\mathrm{i}) = d(S_\mathrm{i})/S_\mathrm{i}$, the uncertainty $\sigma_\mathrm{i} = \sigma(S_\mathrm{i})/S_\mathrm{i} = 1/\mathrm{SNR_i}$ is the channel noise divided by the source flux density, or the reciprocal of the channel SNR. Thus σ_i is dimensionless and is not the same as the usual channel noise in μJy beam^{-1}. The spectral channel weights $W_\mathrm{i} = 1/\sigma_\mathrm{i}^2$ that optimize the least-squares fit depend on the individual source spectrum in addition to instrumental parameters—the least-squares fit automatically determines the optimum channel weights for each source spectral index.

The coefficients a and b of the least-squares fit are (Bevington 1969)

$$a = \frac{1}{\Delta}\left(\sum \frac{x_\mathrm{i}^2}{\sigma_\mathrm{i}^2} \sum \frac{y_\mathrm{i}}{\sigma_\mathrm{i}^2} - \sum \frac{x_\mathrm{i}}{\sigma_\mathrm{i}^2} \sum \frac{x_\mathrm{i} y_\mathrm{i}}{\sigma_\mathrm{i}^2}\right) \tag{36}$$

and

$$b = \frac{1}{\Delta}\left(\sum \frac{1}{\sigma_\mathrm{i}^2} \sum \frac{x_\mathrm{i} y_\mathrm{i}}{\sigma_\mathrm{i}^2} - \sum \frac{x_\mathrm{i}}{\sigma_\mathrm{i}^2} \sum \frac{y_\mathrm{i}}{\sigma_\mathrm{i}^2}\right) \ , \tag{37}$$

where

$$\Delta = \sum \frac{1}{\sigma_\mathrm{i}^2} \sum \frac{x_\mathrm{i}^2}{\sigma_\mathrm{i}^2} - \left(\sum \frac{x_\mathrm{i}}{\sigma_\mathrm{i}^2}\right)^2 \tag{38}$$

and all summation indices go from $i = 1$ through $i = N$. The variances of the fitted a and b values are

$$\sigma_a^2 = \frac{1}{\Delta} \sum \frac{x_\mathrm{i}^2}{\sigma_\mathrm{i}^2} \tag{39}$$

and

$$\sigma_b^2 = \frac{1}{\Delta} \sum \frac{1}{\sigma_\mathrm{i}^2} \ . \tag{40}$$

It is advantageous to use the weighted harmonic mean frequency $\bar{\nu}_\mathrm{h}$ defined by

$$\ln(\bar{\nu}_\mathrm{h}) = \sum W_\mathrm{i} \ln(\nu_\mathrm{i}) \Big/ \sum W_\mathrm{i} \tag{41}$$

as the fiducial frequency ν_0 because

$$\sum W_\mathrm{i} \ln(\bar{\nu}_\mathrm{h}) = \sum W_\mathrm{i} \ln(\nu_\mathrm{i}) \tag{42}$$

$$\sum W_\mathrm{i} [\ln(\nu_\mathrm{i}) - \ln(\bar{\nu}_\mathrm{h})] = \sum W_\mathrm{i} \ln(\nu_\mathrm{i}/\bar{\nu}_\mathrm{h}) = \sum W_\mathrm{i} x_\mathrm{i} = 0 \ , \tag{43}$$

leads to

$$\sum \frac{x_\mathrm{i}}{\sigma_\mathrm{i}^2} = 0 \ . \tag{44}$$

Equation 44 simplifies Equations 36, 37, and 38 to

$$a = \frac{1}{\Delta} \left(\sum \frac{x_\mathrm{i}^2}{\sigma_\mathrm{i}^2} \sum \frac{y_\mathrm{i}}{\sigma_\mathrm{i}^2} \right) \tag{45}$$

and

$$b = \frac{1}{\Delta} \left(\sum \frac{1}{\sigma_\mathrm{i}^2} \sum \frac{x_\mathrm{i} y_\mathrm{i}}{\sigma_\mathrm{i}^2} \right) \ , \tag{46}$$

where

$$\Delta = \sum \frac{1}{\sigma_\mathrm{i}^2} \sum \frac{x_\mathrm{i}^2}{\sigma_\mathrm{i}^2} \ . \tag{47}$$

Equations 39 and 40 simplify to

$$\sigma_a^2 = \left(\sum \frac{1}{\sigma_\mathrm{i}^2} \right)^{-1} \tag{48}$$

and

$$\sigma_b^2 = \left(\sum \frac{x_\mathrm{i}^2}{\sigma_\mathrm{i}^2} \right)^{-1} \ . \tag{49}$$

Even more importantly, Equation 44 makes a proportional to the weighted y_i terms and eliminates the weighted cross-correlation terms $x_\mathrm{i} y_\mathrm{i}$ (compare Equation 36 with 45). Similarly, comparing Equation 37 with 46 shows that b is proportional to the weighted $x_\mathrm{i} y_\mathrm{i}$ terms and free of the the weighted y_i terms. That is, the weighted harmonic mean frequency $\bar{\nu}_\mathrm{w}$ of the data is the unique "pivot" frequency at which the intercept (the fitted $\ln[S(\nu_0)]$) and slope (the fitted α) are uncorrelated. It is the frequency at which the fitted source flux density has the highest SNR. The pivot frequency $\nu_0 = \bar{\nu}_\mathrm{h}$ is plotted as a function of α for the VLASS (2 GHz $< \nu <$ 4 GHz) in the top panel of Figure 4.

For convenience, and with no loss of generality, assume that the spectral channels are uniformly spaced in $x_\mathrm{i} = \ln(\nu_\mathrm{i}/\nu_0)$; that is, channel bandwidth $B_\mathrm{i} \propto \nu_\mathrm{i}$. For a pointed

observation, the integration time τ is independent of frequency, so the channel rms noise is proportional to $B_{\rm i}^{-1/2} \propto \nu_{\rm i}^{-1/2}$. For sources with flux densities proportional to $\nu^{-1/2}$ ($\alpha = -0.5$), $\sigma_{\rm i} \propto {\rm SNR}_{\rm i}^{-1}$ will be the same for all channels. For survey observations with $\tau_{\rm i} \propto \nu_{\rm i}^{-2}$, the channel rms noise is proportional to $(B_{\rm i}\tau_{\rm i})^{-1/2} \propto \nu_{\rm i}^{-1/2} \cdot \nu_{\rm i}^{+1} \propto \nu_{\rm i}^{+1/2}$, and sources with $\alpha = +0.5$ will have $\sigma_{\rm i}$ the same for all channels. For these special cases, the ratio of Equations 48 and 49 is

$$\left(\frac{\sigma_{\rm a}}{\sigma_{\rm b}}\right)^2 = \sum x_{\rm i}^2 \Big/ \sum 1^2 \ . \tag{50}$$

In the limit of large N, sums can be replaced by integrals over x and Equation 50 becomes

$$\left(\frac{\sigma_{\rm a}}{\sigma_{\rm b}}\right)^2 \rightarrow \frac{\int x^2 dx}{\int dx} = \frac{x^3}{3}\Big|_{-l/2}^{+l/2} \Big/ \ x\Big|_{-l/2}^{+l/2} = \frac{l^2}{12} \ , \tag{51}$$

where $l = \ln(\nu_{\rm max}/\nu_{\rm min})$ is the logarithmic width of the full frequency band (Equation 31) and 1/12 is the variance of a unit rectangle. Let $S_{\rm f} = S(\bar{\nu}_{\rm h})$ be the fitted flux density and ${\rm SNR}_{\rm f}$ be the signal-to-noise ratio of the linear fit. Then $\sigma_{\rm a} = \sigma(\bar{S}_{\rm w})/\bar{S}_{\rm w} = 1/{\rm SNR}_{\rm f}$, $\sigma_{\rm b} = \sigma_\alpha$ is the rms error in the fitted spectral index, and

$$\sigma_\alpha \times {\rm SNR}_{\rm f} = \frac{\sqrt{12}}{\ln(\nu_{\rm max}/\nu_{\rm min})} \tag{52}$$

In the case of the VLASS with $\nu_{\rm max}/\nu_{\rm min} = 2$,

$$\sigma_\alpha \times {\rm SNR}_{\rm f} = \frac{\sqrt{12}}{\ln(2)} \approx 5.0 \tag{53}$$

for the special case of a source with $\alpha = +0.5$. Likewise for a pointed S-band observation of a source with $\alpha = -0.5$. For other spectral indices, the channel weights are not equal and the product $\sigma_\alpha \times {\rm SNR}_{\rm f}$ is slightly larger, as shown in the bottom panel of Figure 4. Roughly speaking, Equation 53 indicates that a source fit ${\rm SNR}_{\rm f} \approx 50$ is needed for the VLASS to measure an in-band spectral index with rms uncertainty $\sigma_\alpha \approx 0.1$. For the EMU frequency limits $\nu_{\rm min} = 1.1$ GHz and $\nu_{\rm max} = 1.4$ GHz, $\sigma_\alpha \times$ ${\rm SNR}_{\rm f} \approx 14.4$. While EMU's required ${\rm SNR}_{\rm f}$ is 2.9× higher than All-Sky's, EMU is about 10× as sensitive as All-Sky, so EMU should be about 3.5× more sensitive than All-Sky for measuring spectral indices of faint sources.

To predict the accuracy of *all* in-band VLASS spectral indices, it is necessary to relate ${\rm SNR}_{\rm f}$ to the SNR of the source on the VLASS image. Again it is easier to work with logarithmic channel widths. In the ith channel,

$$(dS_{\rm i})^2 = \left(\frac{\nu_{\rm i}}{\bar{\nu}}\right)^2 \left(\frac{\nu_{\rm i}}{\bar{\nu}}\right)^{-1} = \left(\frac{\nu_{\rm i}}{\bar{\nu}}\right)^1 \tag{54}$$

so

$$\left(\frac{dS_{\rm i}}{S_{\rm i}}\right)^2 = \left(\frac{\nu_{\rm i}}{\bar{\nu}}\right)[S(\bar{\nu})]^{-2}\left(\frac{\nu_{\rm i}}{\bar{\nu}}\right)^{-2\alpha} = {\rm SNR}_{\rm i}^{-2} \tag{55}$$

$${\rm SNR}_{\rm i}^2 = [S(\bar{\nu})]^2\left(\frac{\nu_{\rm i}}{\bar{\nu}}\right)^{2\alpha-1} \tag{56}$$

$${\rm SNR}_{\rm f}^2 = \sum_{\rm i=1}^{\rm N} {\rm SNR}_{\rm i}^2 = [S(\bar{\nu})]^2 \sum_{\rm i=1}^{\rm N}\left(\frac{\nu_{\rm i}}{\bar{\nu}}\right)^{2\alpha-1} \tag{57}$$

Replacing the sum over channels by an integral over $\ln(\nu)$ gives

$${\rm SNR}_{\rm f}^2 = [S(\bar{\nu})]^2 \int \left(\frac{\nu}{\bar{\nu}}\right)^{2\alpha-1} d\ln\nu \Big/ \int d\ln\nu \tag{58}$$

$${\rm SNR}_{\rm f}^2 = \frac{[S(\bar{\nu})]^2}{\bar{\nu}^{2\alpha-1}} \int \nu^{2\alpha-2} d\nu \Big/ \ln(\nu_{\rm min}/\nu_{\rm max}) \tag{59}$$

$${\rm SNR}_{\rm f} = [S(\bar{\nu})]^2 \left(\frac{\nu_{\rm max}^{2\alpha-1} - \nu_{\rm min}^{2\alpha-1}}{2\alpha-1}\right)\left[\frac{\bar{\nu}^{(1-2\alpha)}}{\ln(\nu_{\rm min}/\nu_{\rm max})}\right], \quad (\alpha \neq +1/2) \tag{60}$$

The source SNR on the weighted image multiplied by σ_α is shown in Figure 5. To yield $\sigma_\alpha = 0.1$, a point source with $\alpha = -0.7$ must have an image SNR ≈ 51. For All-Sky, with $\sigma_{\rm w} \approx 65\,\mu$Jy beam^{-1}, the minimum point-source flux density is $S(2.682\ {\rm GHz}) \approx 3.3$ mJy. *Thus All-Sky alone is about twice as sensitive as the combination of WENSS and NVSS* [$S(2.682\ {\rm GHz}) \approx 6.0$ mJy] *for measuring spectral indices of point sources with* $\alpha \sim -0.7$. *EMU alone is about* $3.5\times$ *as sensitive as All-Sky.* These conclusions are actually true for any value of the required accuracy so long as $\sigma_\alpha \ll 1$, not just for the example of $\sigma_\alpha = 0.1$.

5. VLASS Performance and Science Applications

The final VLASS proposal (SSG 2015) lists six VLASS science themes (Imaging Galaxies Through Time and Space, Radio Sources as Cosmological Probes, Hidden Explosions, Faraday Tomography of the Magnetic Sky, Peering Through Our Dusty Galaxy, and Missing Physics) and their goals in Section 3 and "additional science enabled by VLASS" in Appendix C. However, the proposal contains little quantitative evidence that VLASS can deliver the proposed science or that the VLASS is the best survey to do so. This section addresses the questions "Can the VLASS do the proposed science?" and "Will it do better than other surveys, EMU in particular?"

5.1. Imaging Galaxies Through Time and Space

The headline topic in this section is "The star-formation history of the Universe," but the surface-brightness sensitivity of All-Sky is not good enough to detect radio emission from most star-forming galaxies (see Equation 4 and Table 1). All-Sky has a lower surface-brightness sensitivity than FIRST. If All-Sky could trace the evolution of star formation at redshifts $z \leq 0.5$ as claimed, why hasn't FIRST already done better? Actually, even FIRST doesn't have the necessary surface-brightness sensitivity, as demonstrated by the fact that the low-redshift 2dFGRS/FIRST sample yields a local luminosity function for star-forming galaxies that is a factor of ten too low (Magliocchetti et al. 2002). The low-resolution NVSS can detect nearby star-forming galaxies (Condon et al. 2002), and the far more sensitive EMU survey was designed to extend those results to higher redshifts.

Section 3.1 of SSG (2015) says "The optimal combination of sensitivity and spatial resolution of VLASS allows the study of the entire AGN population from classical radio-loud sources down to the realm of radio-quiet AGNs ($P \sim 10^{22-23}$ W Hz^{-1}) ... from $z \sim 0 - 6$." However, a source with $P = 10^{23}$ W Hz^{-1} and $\alpha = -0.7$ at $z = 6$ has a flux density $S = 0.4\,\mu$Jy, well below the Deep point-source detection limit $S_{\rm p} = 7.5\,\mu$Jy beam^{-1}. Deep could not detect such a point source beyond $z \approx 1.6$, and the redshift limit for an extended source is even lower.

To answer its question "Why are some AGN strong radio emitters and others not?", SSG (2015) points out that "better demographics ... are key." To highlight the impact the high-resolution All-Sky survey will have on quasar science, Section 4.1.3 of SSG (2015) cites the Hodge et al. (2011) survey of Stripe 82 to suggest that All-Sky will yield far better demographics than FIRST, noting "The FIRST survey detects barely 10% of SDSS quasars..." while "Hodge et al. (2011) report on A-array observations (i.e., with better resolution than FIRST) to 3× the depth of FIRST in SDSS Stripe-82 and found that 97% of known SDSS quasars are recovered in the higher resolution data."

Hodge et al. (2011) didn't actually detect 97% of the SDSS quasars in Stripe 82, which would have been a huge jump over "barely 10%." The qualifier "known SDSS quasars" apparently means "only the subset of SDSS radio quasars previously detected by FIRST." Section 9 of Hodge et al. (2011) reports "... the FIRST catalog matches to 229 out of 3885 quasars from the SDSS DR7 Quasar Catalog (Schneider et al. 2010) within a matching radius of 5″. Of those, the Stripe 82 catalog recovers 223. In addition to those 223, the new catalog also has radio sources matching 76 quasars not previously detected by FIRST. The total fraction of spectroscopic quasars that are radio sources to the depth probed here is therefore 7.7% (±0.4%)." Thus in Stripe 82 Hodge et al. (2011) recovered 223/229 = 97% of the SDSS radio quasars previously detected by FIRST, but the 3× higher resolution and

3× higher point-source sensitivity of the Hodge et al. (2011) A-array images increased the radio detection rate of all SDSS Strip 82 quasars from 5.9% to 7.7%. This 30% increase is consistent with independent observations (Condon et al. 2013) showing that optically selected quasars have extremely flat source counts. All-Sky is less sensitive than Hodge et al. (2011), so it probably won't improve the quasar detection rate by even 30%.

The "Quasar Science" section in SSG (2015) notes that surface density of optically selected quasars is low and then claims that "Efficient matching of radio sources to surveys at other wavelengths (particularly in the optical) requires $\sim$ arcsec resolution." Not so. Matching radio sources having low surface density (e.g., ~ 290 deg^2 for All-Sky) with quasars not having significantly higher surface densities (~ 40 deg^2 was quoted) requires only that the the synthesized beam solid angle be much smaller than $(290 \text{ deg}^{-2})^{-1}$, or $\theta \ll 200''$ resolution. Even the low-resolution NVSS ($\theta = 45''$) has efficiently matched radio sources to optically selected quasar samples (Condon et al. 2013). EMU's "poor" resolution ($\theta = 10''$) is more than adequate for efficient, reliable, and complete matching with any foreseeable sample of optically selected quasars (see Section A.2), and EMU's 10× higher point-source sensitivity than All-Sky's ensures that EMU will be the preferred survey for detecting radio emission from more optically selected quasars.

"To investigate quasars as a function of orientation, we need robust spectral indices." (SSG 2015). All-Sky "internal" S-band spectral indices are robust only for fairly strong sources [$S(2.682 \text{ GHz}) > 3.3$ mJy], many of which are so extended that All-Sky will not be able to measure their flux densities accurately (Condon et al. 2013). EMU will be able to measure spectral indices of quasars about a factor of 3.5 fainter (Section 4.2).

The key to statistical studies of galaxies through time and space is indeed demographics. Evolving populations of extragalactic radio sources span a wide range of flux densities, angular sizes, surface brightnesses, and redshifts. Unbiased demographics requires flux-limited samples not biased against sources with large angular sizes or low surface brightnesses, a problem for the VLASS. Radio demographers have known for decades that any single survey is dominated by sources near the survey sensitivity limit, so "wedding cake" surveys with several layers of different sensitivity and sky coverage are needed to obtain statistically useful samples spanning the range of source flux densities. The VLASS "wedding cake" shown in Figure 1 is clearly not optimized for studying galaxies through time and space. If that is a primary science goal of the VLASS, the VLASS should be redesigned.

5.2. Radio Sources as Cosmological Probes

The high angular resolutions of Deep ($\theta \approx 0\farcs9$ in the two northern fields and $\approx 2\farcs2 \times 0\farcs9$ in the southern ECDFS field) are comparable with the typical angular size ϕ of faint ($\geq 10\,\mu$Jy) galaxies. The angular-size distribution of such faint galaxies is not well known, and the median angular size of μJy radio sources may range from $\langle\phi\rangle \approx 0\farcs5$ to $1\farcs2$. Detecting most faint galaxies to measure their two-point correlation function or luminosity function requires that the beam be larger than the galaxies, while resolving most galaxies to probe dark energy by measuring weak gravitational lensing shear requires that the beam be smaller than the galaxies.

The resolution, point-source sensitivity, and sky coverage of Deep are only marginally sufficient to exploit the "unique and powerful added value [offered by the radio band] to the field of weak lensing." Section 3.2 of SSG (2015) forthrightly portrays Deep as a pilot survey "...aimed at delivering a 5σ detection of cosmic shear in the radio." Chang et al. (2004) made a 3.6σ detection using FIRST, while "Current optical weak lensing surveys ...are expected to deliver detections with a significance of 15, 30, and $43\,\sigma$, respectively." The main value of Deep will be to study radio systematics in preparation for possible SKA surveys with much higher sensitivity and wide sky coverage.

Figure 2 of SSG (2015) shows the accuracy with which luminosity functions of star-forming galaxies near $z = 1$ and $z = 3$ can be determined by 3 GHz continuum surveys covering 2, 4, and 10 deg^2 with a common detection limit $S = 7.5\,\mu$Jy. The detection limit of Deep is $S_{\rm p} = 7.5\,\mu$Jy beam^{-1}, not $S = 7.5\,\mu$Jy. The 3 GHz resolution of Deep is about $0\farcs8$, so Deep will miss most star-forming galaxies with angular diameters $\phi > 0\farcs8$, as shown in Section 4.1.5. The ability of Deep to match the luminosity functions shown Figure 2 of SSG (2015) and the effects of resolution bias is unknowable until the angular-size distribution of μJy sources is specified and taken into account.

5.3. Hidden Explosions

Radio transients often signal explosive events, and Section 3.3 of (SSG 2015) points out that "the most numerous radio transients with the greatest potential impact are actually those populations that have been hidden from view at these other wavebands, being largely detectable only at radio wavelengths." Multi-epoch blind radio surveys are needed to find them. All-Sky will cover $\Omega \approx 3.4 \times 10^4$ deg^2 of the sky $N = 3$ times over a span of seven years (once every 32+ months), and each epoch will have an rms noise $\sigma_{\rm e} \approx \sigma_{\rm n} N^{1/2} \approx 69\,\mu$Jy beam$^{-1} \times 3^{1/2} \approx 120\,\mu$Jy beam^{-1}, which is $\approx 120\,\mu$Jy for unresolved transient sources.

The transient detection limit must be a fairly high $S \approx 10\sigma_e \approx 1.2$ mJy because there are $\approx 10^{11}$ synthesized beams in $N\Omega \approx 10^5$ deg^2. Figure 5 of (SSG 2015) shows the extragalactic transient "phase space" (estimated instantaneous areal density ρ of transients stronger than flux density S as a function of S). On it, a survey covering solid angle Ω with detection limit S in each of N epochs is characterized by the point at $S = 10\sigma_e = 10\sigma_n N^{1/2}$, $\rho = (N\Omega)^{-1}$.

The product $S^2\rho = 100\,\sigma_n^2/\Omega$ of any given survey (fixed telescope, frequency, and total observing time) is independent of the number of epochs N, so changing N moves the survey parallel to the diagonal going from the upper left to lower right on Figure 5 of SSG (2015). A simple figure-of-merit for comparing transient surveys is $M \equiv (\Omega/\sigma_n^2)$. By this criterion, All-Sky is three or four orders-of-magnitude better than the other transient surveys plotted on Figure 5. EMU covers $\Omega \approx 3.1 \times 10^4$ deg^2 with rms noise $\sigma_n \approx 10\,\mu$Jy beam^{-1}, so its transient figure-of-merit is about 40× higher than All-Sky's.

The dashed line on (SSG 2015) Figure 5 shows the areal density of the usual variable but persistent extragalactic radio sources that must be distinguished "genuine" transients. The areal density of variable sources is $\sim 10^5$ above the All-Sky point and even farther above the EMU point. To exploit the full potential of these surveys, it will be necessary to find the one transient needle in a haystack of $\sim 10^5$ variable straws plus the large expected number of transient "sources" stronger than $10\sigma_e$ that are actually sidelobes in the All-Sky snapshot images. This will be difficult, especially for surveys with low N, so I suspect that neither survey will perform as well as indicated by Figure 5, and that the apparent advantage of EMU over All-Sky will be much less than 40× unless EMU, with its much larger field-of-view, can be scheduled to yield $N \gg 3$ epochs.

5.4. Faraday Tomography of The Magnetic Sky

The drivers of All-Sky polarization science are "to characterize properties of the magneto-ionic medium in AGNs and in galaxies across a wide range of redshifts" and "the use of the VLASS [All-Sky] for studies of Faraday foregrounds" with "a 6-fold increase in the background polarized source densities" available today from the NVSS. The proposal doesn't compare this All-Sky prediction with the more sensitive EMU. These two surveys are complementary in the sense that the 3 GHz All-Sky can penetrate much higher Faraday depths than the 1.4 GHz EMU, which has higher Faraday resolution.

The polarization science section of SSG (2015) conflates polarized flux density and polarized brightness. The statements "At the angular resolution of the VLASS [All-Sky], most objects in the mJy regime will be resolved allowing tomographic exploration of the

structure of AGN and radio galaxies, ..." and "Based on the NVSS we expect over 10^5 sources with polarized fluxes > 0.75 mJy ..." are actually in conflict. Detection rates are limited by image brightness in mJy beam^{-1}, not by flux density in mJy. If most objects are resolved by All-Sky, the All-Sky detection rate will be much lower than calculated from polarized flux densities measured with the low-resolution NVSS. The statement "Average fractional polarization of unresolved Milky-Way type galaxies is a factor of 3–4 higher at 2 GHz than at 1.4 GHz (Stil et al., 2009; Braun et al., 2010; Sun & Reich, 2012), a 2–4 GHz survey with sufficient sensitivity thus opens enormous potential for characterizing the development of galactic magnetic fields" suggests that the VLASS can detect polarization from Milky-Way type galaxies despite the fact that it doesn't even have the surface-brightness sensitivity to detect Milky-Way type galaxies in total intensity. Figure 8 of SSG (2015) shows the redshift and luminosity distributions of galaxies "expected to be detected in one square degree with polarized flux density greater than $10\,\mu$Jy." The detection limit of Deep is not $< 10\,\mu$Jy, it is $< 10\,\mu$Jy beam^{-1}. Deep will heavily resolve and hence not detect polarization in most of the low-redshift or low-luminosity galaxies plotted.

5.5. Peering Through Our Dusty Galaxy

The headline Galactic science in SSG (2015) Section 3.5 is discovering exotic radio pulsars, where "The value of the VLASS is that it will serve as a finding survey in which *candidate radio pulsars* can be used to winnow the large number of radio sources detected in the VLASS to a feasible number on which to conduct a periodicity search." Of the $\rho \sim 380$ sources deg^{-2} with flux densities above the All-Sky *peak* flux-density limit, between 25% and 50% will be resolved by All-Sky, leaving $\rho \sim 240 \pm 50$ deg^{-2} point sources as pulsar candidates.

Winnowing is efficient to the extent that it can easily reduce the sky density of candidates well below one per primary beam solid angle of the telescope used for the periodicity search. In the case of the GBT, $\Omega_{\rm pb} \approx [20/\nu({\rm GHz})]^2$, or $\rho \ll 13$ deg^{-2} ($\rho \ll 2.5$ deg^2) at 820 MHz (350 MHz), the pulsar search frequencies most often used at the GBT. However, SSG (2015) claims only "With a combination of multi-wavelength counterpart comparisons, polarization, future high angular resolution observations, and other criteria, we expect it to be feasible to reduce the source density to of order 30 deg^2."

Even efficient winnowing doesn't help if the radio candidate catalog isn't deep enough to match the periodicity search sensitivity. In the SSG (2015) example of identifying new γ-ray pulsars in the FERMI catalog (Ray et al. 2012), it turns out that none of the new pulsars would have been seen by All-Sky because all are a factor of 5 or more below the

All-Sky detection limit at 3 GHz. Part of the problem for the 3 GHz All-Sky is that pulsars have much steeper radio spectra ($\alpha \sim -1.6$) than most radio sources ($\alpha \sim -0.7$), so high-frequency surveys have low needle/haystack ratios.

Section 3.5 of SSG (2015) covers All-Sky detections of radio stars. *Detecting* radio stars in our Galaxy is fairly easy, but reliably *identifying* them (Section A.2) requires extremely accurate positions because the fraction f of all radio sources that are powered by stars is very small ($f < 10^{-4}$). All-Sky really should greatly improve on existing flux-limit samples of radio stars, even though it is not much more sensitive than FIRST or NVSS, because its high angular resolution allows it measure accurate ($\sigma \sim 0\farcs3$ in each coordinate) positions of even the faintest detectable point sources. It has little competition from FIRST, which does not cover the Galactic Plane, from the NVSS, whose position errors are too large, or possibly even from EMU, which may be confusion limited near the Galactic Center. More weight should have been given to this part of the All-Sky proposal.

Section 3.5 notes that "...the total number of known [planetary] nebulae is far lower than even the most conservative expectations. Consequently, large samples of these objects are required to trace evolutionary sequences." Although the proposal explicitly recognizes the need for adequate brightness temperature sensitivity, it uses the Aaquist & Kwok (1990) $\lambda = 6$ cm VLA survey of PNe to estimate that PNe tend to be a few to several arcseconds in size. The Aaquist & Kwok (1990) survey is strongly biased against detecting extended, low-brightness PNe because it targeted an optical sample of PNe smaller than $\phi \sim 4''$ and was made with $\theta = 0\farcs4$ resolution. By comparing the IRAS colors of their radio-detected PNe with those of evolved PNe, Aaquist & Kwok (1990) concluded that they had "...identified a group of nebulae with high radio surface brightness temperatures which are excellent candidates for young planetary nebulae." The typical PN is about 0.3 pc in diameter, or about $\phi \approx 8''$ at the distance of the Galactic center. To trace evolutionary sequences of PNe, a radio survey should have resolution $\theta > \phi$. With $\theta \approx 2\farcs8$, All-Sky will detect a $\phi \approx 8''$ PN only if it is stronger than $S \approx 3$ mJy, which makes it no more sensitive than the NVSS survey of PNe (Condon & Kaplan 1998) and far less sensitive than EMU.

Figure 9 in SSG (2015) is a logarithmic plot showing relative sensitivities in the L, S, C, and Ku bands to sources with different spectral indices, *normalized to 2.8 GHz*, the S-band logarithmic mean frequency. In general, nonthermal sources are stronger at lower frequencies and thermal sources are stronger at higher frequencies. The caption concludes "The Galactic radio source population contains both thermal and non-thermal emitters, and the 2-4 GHz observing frequency range for the VLASS provides a balance in the sensitivity for these two classes of sources." Not so. The "balance" apparently provided by observing in the 2–4 GHz frequency range is an artifact generated the choice of 2.8 GHz as the normalizing frequency,

and has nothing to do with actual populations of Galactic sources. Likewise, the claim in Section 3.5 "Thus, observation frequency of 2–4 GHz, as planned for the VLASS, balances sensitivity to thermal and non-thermal sources, both of which are found in Galactic radio source populations." is without foundation. Both Figure 9 and the claim in Section 3.5 should be deleted from the proposal.

5.6. Angular Resolution and Optical Identifications

The main drawback of All-Sky is its poor brightness sensitivity, which is the inevitable consequence of its unusually high angular resolution, $\theta \approx 2\farcs8$. The point-source detection limit of All-Sky is $S \approx 350\,\mu$Jy, but so many sources have angular diameters $\phi > \theta \approx 2\farcs8$ that All-Sky will generate incomplete and biased samples of most source populations. All-Sky will detect nuclear starburst galaxies like Arp 220 but completely miss normal star-forming galaxies. All-Sky will detect young PNe but miss most older PNe. All-Sky will detect compact sources in radio galaxies and quasars, but it will miss most of the flux from jets and lobes larger than their host galaxies because there is *no* redshift at which sources larger than 24 kpc have angular diameters smaller than $2\farcs8$.

All-Sky was forced to such high angular resolution by the claim in Section 4.1.1 and Appendix D of SSG (2015) that $> 95\%$ reliable position-coincidence identifications with optically faint galaxies can be made if and only if θ is very small, regardless of source signal-to-noise ratio S/N. That claim is based on a bad identification method that tries to match the individual components of a resolved double source, instead of the source centroid, with its host optical galaxy. For example, the radio source Cyg A has two strong lobes, each about 1 arcmin from the host optical galaxy. Matching each lobe to a deep optical catalog will yield two bad "matches" with radio/optical separations ~ 1 arcmin. The problem of mis-identifying individual lobes of double sources has been addressed by "collapsing" close pairs of radio components into a single component whose centroid position is much closer to the optical galaxy. Lindsay et al. (2014) tried this and found "when matching collapsed FIRST sources or NVSS sources directly to the optical catalogues, we find no evidence of a significant difference between the results." That is, the high resolution ($\theta = 5\farcs4$) of FIRST and the low resolution ($\theta = 45''$) of NVSS give identification results on extended sources that are not significantly different.

Only in the rare cases that the high-resolution survey can detect and resolve a weak radio core does a high-resolution survey do better. Surveys such as EMU with lower resolution but higher sensitivity will yield identifications of most sources that are at least as reliable as All-Sky's. Appendix A below presents a detailed review of what went wrong in SSG (2015)

Appemdix D.

The ideal radio survey would yield flux-limited source samples with optical identifications that are *complete* as well as reliable. All-Sky optical identifications are necessarily $> 25\%$ incomplete because All-Sky radio catalogs are $> 25\%$ incomplete. This problem is not addressed by SSG (2015). Incompleteness is worse than unreliability because it cannot be corrected by follow-up observations. I expect that EMU will yield more useful optical identifications of flux-limited samples than All-Sky will.

6. Justifying the VLASS

The VLASS must have a strong justification for its request for about 9,000 hours of valuable time on the new JVLA. It needs to be justified as (1) being technically better (e.g., more sensitive, higher position accuracy, ...) than other surveys and (2) having a higher "reach" or impact than the regular proposals it would displace on the VLA schedule.

Read the "Report of the NRAO Large Proposals Committee" (Bridle et al. 1997) of the committee created specifically to address the competition between large surveys and smaller PI observations, especially their Recommendation 7 "The NRAO should not make Announcements of Opportunity for the submission of large proposals. Large proposals should be submitted at the normal proposal deadlines, without special solicitation by the observatory." The reasoning behind that recommendation (Bridle et al. 1997) is (emphases added):

"The committee considered whether the NRAO should explicitly solicit proposals for large projects via Announcements of Opportunity, targeted either to specific disciplines or to special deadlines (other than those of the regular proposal process.)

"It was our unanimous opinion that this would be undesirable. It would separate "opportunities" for proposing large projects from the regular proposal process, whereas we see merit in keeping the processes for large and small proposals well-coupled. *It is also hard to see what benefit would come by encouraging the whole user community to think about large proposals simultaneously.*

"The NRAO-operated telescopes are ground-based and flexible in their capabilities, so operational and planning considerations differ greatly from those needed to establish the scientific program of space-borne instruments, for example. *The AO approach would however place some obligation on the NRAO to schedule some large projects after a period in which it had encouraged the whole user community to make proposals for them.*

"It is particularly undesirable to create an artificial imbalance between the pressures for

large and regular proposals when our ultimate goal is to find an appropriate balance. *We believe that balance is more likely to be achieved through a proposal process that is driven mainly by the scientific interests of individual investigators, rather than through one driven by ad hoc deadlines*."

6.1. The Better Mousetrap

FIRST and NVSS are prototypes for the All-Sky survey. They were justified primarily on the basis of their orders-of-magnitude technical superiority over previous large-scale sky surveys, and not on any specific "transformational science" (the 20th century term for today's "killer app") they would accomplish. Rather, the bulk of the science would be done by community users who would come up with new ideas to exploit the greatly improved survey data—build a better mousetrap, and the world will beat a path to your door. The original FIRST paper (Becker et al. 1995) could legitimately claim that "FIRST represents a factor of ~ 50 improvement in limiting sensitivity over the best available sky survey at any radio wavelength" and "More importantly, however, FIRST also represents a factor of 50 improvement in angular resolution and concomitant positional accuracy." Of course, to be valuable to the general scientific community, it also has to cover a large part of the sky; FIRST would be "in short, the radio equivalent of the Palomar Sky Survey for 25% of the celestial sphere."

Similarly, the primary selling point for the EMU (Extragalactic Map of the Universe) survey covering the sky south of $\delta = +30°$ (75% of the celestial sphere) with $\sigma \approx 10\,\mu$Jy beam^{-1} rms noise and $\theta = 10''$ resolution was that "EMU has the potential to have the enormous impact that the NVSS had a decade ago, but at a factor of 40 better in sensitivity and 5 in angular resolution."

Unfortunately, All-Sky is only $\sim 1.5\times$ as sensitive to point sources as FIRST, and it is less sensitive to extended sources. Neither All-Sky nor Deep have the surface-brightness sensitivity to detect the extended radio emission from most spiral galaxies. EMU combines the best features of both FIRST (high point-source sensitivity and the angular resolution to identify weak sources with faint galaxies) and NVSS (high surface-brightness sensitivity and nearly "all sky" coverage). The instantaneous sky coverage of EMU (30 deg^2) beats All-Sky by more than two orders-of-magnitude, so EMU will be a superior finder of bright transients. Finally, EMU is likely to be completed at about the same time scale as the VLASS (2023) because ASKAP will become a dedicated survey telescope after the second-generation array feeds are installed. All of the second-generation feeds have now been funded for construction during the next two years, and the EMU survey itself only needs two years for completion,

compared with seven years for the VLASS. It doesn't matter which survey wins the race to completion by a year or two; the impacts of large surveys like FIRST and NVSS, VLASS and EMU are felt on time scales of decades.

The Deep survey *is* a better mousetrap for point sources, with $\sigma \approx 1.5\,\mu$Jy beam^{-1} and $\theta \approx 0\farcs8$ resolution, specifications that EMU and WODAN will never reach. Deep covers only a tiny fraction of the sky ($\Omega = 10$ deg$^2 \approx 0.024\%$ of the sky), so it is analogous to the various "deep" surveys by Hubble, Chandra, and Spitzer. If Deep is done at 3 GHz with the A configuration, it will partially resolve most faint star-forming galaxies. This is good for studying the shear produced by weak gravitational lensing but bad for obtaining the complete samples of low-brightness sources needed for studying the evolution of star formation. Equation 5 indicates that Deep could detect most star-forming galaxies if its beamwidth were at least $\theta \approx 2\farcs8$, which is possible with the B configuration at either 3 or 1.4 GHz.

The high scientific impact of the very sensitive multi-band optical/IR Hubble Deep Fields comes from the fact that they really are "deep" in the sense of detecting and distingiushing galaxies at very high redshifts. In contrast, the median redshift of radio sources is nearly independent of flux density, so more sensitive radio surveys like Deep mainly detect $z \sim 1$ sources with lower radio luminosities (Condon 1989). Also, there is no radio spectral signature that clearly distinguishes high-redshift sources. The most distant quasars may already be in the FIRST and NVSS catalogs, but we have to way to distinguish them from the millions of "ordinary" radio sources. High-redshift starburst galaxies stand out only at sub-mm wavelengths, where they appear frequently as background sources in ALMA images. A Deep proposal for 3,000+ hours of JVLA time to constrain the evolution of star formation out to $z \sim 1$ or 2 needs strong and *quantitative* scientific and technical justifications. In particular, the angular resolution needs to be lowered and the "Prussian hat" VLASS wedding cake (Figure 1) needs more layers to optimize coverage in that part of the the redshift-luminosity plane containing the galaxies responsible for the bulk of star formation.

6.2. "Reach" or Citation Impact

Appendix A.2 of Murphy et al. (2014b) and Appendix B.2 of SSG (2015) use the citation rates of the FIRST survey paper (Becker et al. 1995), the FIRST catalog paper (White et al. 1997), and the NVSS paper (Condon et al. 1998) to estimate the scientific impact of future large surveys like All-Sky. The ADS citation histories of these papers as of 2014 September 23 are shown in Figure 6. Although these publications are now 16 to 19 years old, their citation rates remain steady or slowly growing, and their combined refereed citation rate is

about ~ 320 per year. No competitive surveys have been published, so their lifetime refereed citation numbers have grown to 1211, 552, and 2466, respectively, for a total of 4229 when all three papers are added up.

The take-home lesson from Figure 6 is that large surveys should be designed for the long run, and surveys that are surpassed after only a few years will have much less impact. It makes no sense to rush the VLASS in order to "scoop" EMU, only to have it surpassed shortly after it is completed.

How does the citation impact of NVSS+FIRST compare with the regular VLA projects that these surveys displaced? Together these two surveys used up about 6,000 hours, or one year of VLA observing time, so their citation numbers should be compared with the citation numbers of papers produced by one year of "regular" VLA projects.

Appendix A.2 of Murphy et al. (2014b) compared the number of refereed VLA papers published per year (192) with the number of refereed citations per year of FIRST and/or NVSS (262) and concluded "Thus, there is very strong evidence against the argument that the science out of the VLA is negatively impacted when surveys displace regular proposals." I think this is comparing apples (number of refereed VLA papers *published* per year) and oranges (number of refereed papers *citing* FIRST and/or NVSS data per year).

The relevant comparison for the number of refereed papers citing FIRST and/or NVSS data per year is the number of refereed papers citing the 192 regular VLA papers per year. For example, if the average number of citations per regular VLA paper per year is 4, the 192 regular VLA papers from one year will result in 768 citations per year. Even more relevant, and more favorable to FIRST and NVSS, is comparing the lifetime number of citations attributable to FIRST/NVSS (4229) with the lifetime number of citations attributable to the 192 regular VLA papers resulting from one year of VLA observing time. I checked with Marsha Bishop, the NRAO librarian, and the lifetime number of citations per VLA paper published in the years 2007-9 is 34, so the 192 regular VLA papers should yield a lifetime number of citations about 6500, which is still somewhat higher than the FIRST/NVSS 4229.

I conclude that citation rates, either per year or integrated over paper lifetime, don't clearly favor FIRST/NVSS over small VLA programs. The JVLA today is in much heavier demand than the VLA was 20 years ago, and the upgrade has helped targeted observations far more than it has helped surveys (Section 4), so the VLASS will need a stronger justification than the citation counts presented in Appendix A.2 of Murphy et al. (2014b) or Appendix B of SSG (2015).

A. Appendix A: Positional Accuracy and Angular Resolution

There is a still-unresolved debate within the SSG (or more specifically, between the SSG and me) about the radio resolution needed to make optical identifications of radio sources with faint galaxies and quasars. See Appendix D of (SSG 2015) for the latest version of the claim that 95% identification *reliability* requires a large search radius $\sim 0.3\,\theta$. This claim is based on a straw-man identification procedure that does not distinguish between radio *components* (peaks on a radio image) and radio *sources* (the totality of radio emission from a galaxy). See Condon (2014), Appendix D of SSG (2015), and this Appendix for the current state of this debate. The identification question needs to be sorted out before the VLASS design is frozen. Also, the VLASS proposal still needs to address the question of identification *completeness*, which decreases at high angular resolution, as the radio survey catalog completeness decreases.

Section 5.1.1 of Murphy et al. (2014b) states that resolution but not sensitivity is a key survey parameter:

"While sky area is one of the two key parameters that define the value of a wide-area radio survey, the other key parameter is resolution, as this allows counterparts to be identified at other wavelengths among the dense populations of faint galaxies."

The reason seems to be the claim in Murphy et al. (2014b) Appendix B that the proper identification search-circle radius is $\sim 0.4\theta$, regardless of (S/N). The more sensitive EMU and WODAN surveys are dismissed as not having sufficient resolution ($10''$ and $15''$, respectively) to make deep optical identifications:

"For Pan-STARRS, a FWHM resolution better than $7''$ is required for 95% reliability in radio-PS1 cross-matches, as demonstrated in Figure 14. That criterion is easily met by VLASS, but with resolutions of $10''$ and $15''$ respectively (FWHM), both ASKAP-EMU and WODAN fall short (Figure 14). Thus, despite their excellent flux sensitivity, the forthcoming SKA-precursor surveys will not have adequate spatial resolution for confident identifications of counterparts in Pan-STARRS.

"A recurring claim is that the excellent $\sim 10\,\mu$Jy rms flux sensitivity planned for the SKA-precursor surveys (WODAN, ASKAP-EMU) will lead to good positional accuracy for radio sources despite the relatively low resolution of those surveys. The evidence, however, suggests that this is incorrect — the positions of radio sources observed at low resolution do *not* actually converge to the optical counterpart position as (S/N) increases. The wrong conclusion is reached due to simplistic assumptions about the structure of radio sources. In Appendix B we provide a detailed discussion and analysis (i.e., the "S/N model of positional accuracy") demonstrating that half of the optical counterparts to SDSS depth will be false

matches using the matching radius that will be required for WODAN (e.g., see Figure 14). The false counterparts will obviously be an even problem for deeper optical surveys, such as the ongoing DES and HSC surveys and eventually for LSST. Thus the SKA-precursor surveys can not be substituted for the VLASS all-sky survey. This tier will have a long, useful, and heavily used lifetime even into the era of the SKA-precursor surveys." (Section 5.1.1)

Likewise for WIDE:
"At the limits of the DES, HSC, and LSST surveys there are 5, 8, and 14 galaxies in an ASKAP beam—never mind the number of stars. The higher S/N observations of EMU/Wodan will not mitigate this source density when it comes to associating optical and radio sources (see the Appendix), resulting in a high probability of misidentifications. B-array observations in the S-band provide sufficient resolution to bring these numbers down to $\lesssim 1$ galaxy in the VLA beam without unnecessarily over-resolving extended radio sources." (Section 5.2)

This Appendix B analysis of angular resolution and optical identifications has serious problems. It
(1) sets up a straw-man "S/N model" that ignores calibration errors when calculating position errors,
(2) knocks down the "S/N model" by introducing a faulty identification technique that seems to imply much larger "empirical" position errors,
(3) incorrectly ascribes these large errors to source asymmetry,
(4) claims that the identification search circle radius must be $\sim 0.4\theta$, regardless of S/N,
(5) dismisses more sensitive but lower resolution surveys as being unable to identify even moderately bright optical objects (e.g., $r = 22.1$ for EMU, $r = 20.7$ for WODAN) with 95% reliability,
(6) emphasizes identification reliability R but omits the equally important identification completeness C that is degraded by high angular resolution, and
(7) ignores the powerful and widely used likelihood-ratio method (Sutherland & Saunders 1992) for improving on position-coincidence identifications.

These problems are addressed in the remainder of Section A.

A.1. Positional Accuracy

A.1.1. The "S/N Model" of Positional Accuracy

Appendix B in Murphy et al. (2014a) presented the straw-man "S/N model" for positions errors and defines it by the rule:

"...as the flux density increases, the positional error will decrease as 1/(S/N), allowing the optical counterpart to be matched. Specifically, the NVSS description (Condon et al. 1998) gives this formula for the noise in RA or Dec for point sources:

$$\sigma_{1D} = \frac{\theta}{(S/N)\sqrt{(2\ln 2)}} \ . \tag{A1}$$

Here θ is the resolution FWHM (45″ for NVSS) and S/N is the signal-to-noise ratio. The median NVSS rms noise for these matched sources is 0.47 mJy/beam. Note that this noise equation already has been increased by an empirical factor of $\sqrt{2}$ compared with the theoretical equation "to adjust the errors into agreement with the more accurate FIRST positions" (Condon et al. 1998). This predicts $\sigma_{1D} \sim 7\farcs6$ at the catalog detection limit (S/N = 5) and $\sigma_{1D} \sim 1''$ at a flux density of 18 mJy/beam."

Equation (3) in Murphy et al. (2014a) Appendix B (Equation A1 here) differs from Equation 25 in Condon et al. (1998) because it confuses S/N with ρ in Equation 25. The value of ρ for point sources given in Equation 26 of Condon et al. (1998) is actually $\rho = \sqrt{2}(S/N)$, so Equation (3) overestimates σ_{1D} by a factor of $\sqrt{2}$. Equation (3) for the noise component of error should read

$$\sigma_{1D} = \left(\frac{1}{\sqrt{2}}\right)\frac{\theta}{(S/N)\sqrt{(2\ln 2)}} \approx \frac{0.6\,\theta}{(S/N)}. \tag{A2}$$

Although presented as "a long-standing notion" needing to be debunked, the straw man "S/N model" was first defined in Appendix B. It is not a long-standing notion because it implies that the *noise component* of position error is the *total* position error used for identifying point sources. In the long-standing "two component" calculation of position errors, the noise component of position error does decrease as 1/(S/N) (Condon 1997), but it is always added quadratically to the calibration component of error, which is independent of (S/N). For example, the actual NVSS description (Condon et al. 1998) is:

"The rms uncertainties (σ_α, σ_δ) in the centroid coordinates (α, δ) of any source with uncorrected peak amplitude A_P can be approximated by quadratic sums of intensity-independent calibration uncertainties (ϵ_α, ϵ_δ) and noiselike uncertainties that are inversely proportional to A_P."

Comparing the "S/N model" 90% confidence errors (shown by the straight blue line in Figure 21 of Appendix B and reproduced here as Figure 9) with the 50% confidence

curves in Figure 30 of Condon et al. (1998) for the total NVSS pointing errors including the calibration errors $\epsilon_\alpha = 0\farcs45$ and $\epsilon_\delta = 0\farcs56$ makes this distinction obvious. The failure of the "S/N model" to match the data points above $S \sim 0.10$ Jy in Figure 9 is caused by its omission of intensity-independent calibration errors.

A.1.2. The "Two Component Model" of Positional Accuracy

To visually fit the dense black band of data points in Murphy et al. (2014a) Figure 9, it is most appropriate to calculate r_{50}, the 50% confidence radial separation between the measured and true positions. For Gaussian-distributed 1D position errors with rms $\sigma \equiv \sigma_{1D}$ in each coordinate, the distribution of 2D position errors is

$$P(r) = \frac{r}{\sigma^2} \exp\left(-\frac{r^2}{2\sigma^2}\right) , \tag{A3}$$

and the cumulative probability that r is less than some cutoff r_c is

$$P(< r_c) = \int_0^{r_c} P(r)dr = 1 - \exp\left(-\frac{r_c^2}{2\sigma^2}\right) . \tag{A4}$$

The median cutoff r_{50} defined by $P(< r_{50}) = 50\%$ should divide the black band of data points into equal numbers above and below. Solving Equation A4 with $P(< r_c) = 0.50$ gives

$$r_{50} = \sqrt{2\ln 2}\,\sigma \approx 1.18\,\sigma \ . \tag{A5}$$

Similarly, the radius of the 90% confidence error circle is $r_{90} = \sqrt{2\ln 10}\,\sigma \approx 2.15\,\sigma$, $r_{95} = \sqrt{2\ln 20}\,\sigma \approx 2.54\,\sigma$, $r_{99} = \sqrt{2\ln 100}\,\sigma \approx 3.03\,\sigma$, etc. ($r_{90}$ here is the counterpart of σ_{90} in Appendix B.)

The NVSS has $\theta = 45''$ resolution, $\sigma_n = 0\farcs45$ mJy beam^{-1} rms noise, and $\epsilon \approx 0\farcs5$ rms calibration errors in each coordinate. Most NVSS sources are unresolved, so the "two component" model for position errors predicts

$$\sigma \approx \left[\left(\frac{0.6\theta}{(S/N)}\right)^2 + (0\farcs5)^2\right]^{1/2} \approx \left[\left(\frac{12''}{S(\mathrm{mJy})}\right)^2 + (0\farcs5)^2\right]^{1/2} . \tag{A6}$$

For all $S \gg 24$ mJy, calibration errors dominate noise errors, so $\sigma \approx 0\farcs5$ and $r_{50} \approx 0\farcs6$, in good agreement with the dense horizontal band of data points in the right half of Figure 9. For $S \ll 24$ mJy, $r_{50} \approx 1.18\,\sigma \approx 14''/S(\mathrm{mJy})$ is noise dominated and inversely proportional to S. Consequently the r_{50} line has the same slope as the blue line in Figure 9, but its intercept at the left edge of the plot (where $S \approx 2$ mJy) is $r_{50} \approx 7''$, which is indeed in the

middle of the black band of data points. This demonstrates that the long-standing "two component" method of calculating position errors fits real data much better than the new "S/N model". The "two component" results for the radius of the NVSS 90% confidence error circle are $r_{90} \approx 1\farcs08$ at high flux densities and $r_{90} \approx 26''/S(\mathrm{mJy})$ at low flux densities.

Sources partially resolved by the NVSS ($\phi \lesssim \theta = 45''$) will appear broader than $45''$ FWHM on NVSS images. In that case, θ in Equation A6 should be replaced by $(\phi^2 + \theta^2)^{1/2}$ and the position error σ will be slightly larger.

A.1.3. The "Empirical" Position Error

The red binned curve in Figure 9 plots the "empirical" 90% confidence FIRST-NVSS separation r_{90} or σ_{90} as a function of flux density. It ranges from $r_{90} \approx 5''$ at the highest flux densities to $r_{90} \approx 20''$ below $S \sim 250$ mJy, much larger than r_{90} predicted for point sources by both the "S/N model" and the "two component" models. What went wrong?

Large, asymmetrical radio sources are blamed in Murphy et al. (2014a) Appendix B:

"**Why are the low-resolution positions so inaccurate?** — Why are the inaccuracies in the positions so much greater than the S/N model predictions? Real radio sources are not symmetrical objects. They have lobes, jets, cores; star-forming galaxies have spiral arms; and there can be confusion where multiple radio sources get mixed together in the low resolution beam. A low resolution survey does indeed provide a measurement, with high accuracy, of the mean flux-weighted position as the S/N increases. However, the flux-weighted centroid is often not where the optical counterpart lies. In many cases, the counterpart is associated with some sharp structure within the radio source, and that structure may be far from the flux-weighted center."

My explanation is that the method used to generate the data points in Figure 9 is a really bad way to match NVSS sources with FIRST sources and leads to bad matches with separations approaching $100''$ that contaminate the FIRST/NVSS separation data. Consequently the red 90% confidence "empirical" curve is not a useful indicator of radio-optical offsets and cannot be used to calculate identification search radii for the NVSS or, more importantly for the VLASS proposal, for surveys that compete with it (EMU, WODAN, and even FIRST).

How were the matches in Figure 9 generated? Appendix B explains:

"As a large-scale test, we selected a sample of all the FIRST sources that have an SDSS match within $0\farcs7$ and that have an NVSS match within $100''$. For all these $\sim 135,000$ sources, we computed the distance to the nearest NVSS source. The important thing about

this sample is that the FIRST source matches the optical source position. That means that if NVSS is to identify the same counterpart, it needs to have a position close to the FIRST source position. There may be several FIRST source components associated with a single NVSS source, but only the FIRST sources that match optical counterparts are included."

The sky density of FIRST sources is ≈ 90 deg^{-2} (White et al. 1997) and the sky density of NVSS sources is ≈ 53 deg^{-2} (Condon et al. 1998), so $\approx 60\%$ of FIRST sources have true NVSS counterparts and $\approx 40\%$ of FIRST sources do not. Among these unmatched FIRST sources, those having no unrelated NVSS neighbors within $100''$ were dropped from the sample. All unmatched FIRST sources having unrelated NVSS neighbors within $100''$ remain in the sample and appear as false identifications with NVSS-FIRST separations up to $100''$. The probability that an unrelated NVSS source lies within $100''$ of a random position on the sky is ≈ 0.13, so we expect about 124,000 good matches and 11,000 bad matches among the 135,000 plotted data points. With only 92% of the matches being good, the "empirical" 90% confidence limit is bound to be too high.

How can we decide between the "bad sources" and the "bad matches" explanations for the large 90% confidence "empirical" errors?

The "bad sources" problem was studied observationally by Fomalont (1969). He found that, even among strong extragalactic sources ($S \geq 2$ Jy at 1.4 GHz), only about 30% would be significantly resolved ($\phi > 45''$) by the NVSS, and most extended sources are fairly symmetric. Among all extended sources, symmetric or not, the offset of the source's *flux-weighted centroid* from the host galaxy was usually within 10% of the overall source extent and never more than 20% (see his Figure 8). Thus the optical identification of a $50''$ source is likely to lie within $5''$ and almost certainly within $10''$ of the source centroid. Any "bad sources" should contribute points centered on and concentrated close to the black band in Figure 9. Very large FIRST-NVSS separations (e.g., $> 70''$) should be *extremely* rare, and they would not normally be accepted as identifications in any case.

In contrast, NVSS "bad matches" should be randomly distributed over $r = 100''$ circles centered on the FIRST sources, and they should contribute about 8% of the data points in Figure 9. The probability that the FIRST/NVSS separation is between r and $r + dr$ should be nearly proportional to r, so the "bad matches" data points should be concentrated near the $r = 100''$ limit at the top of Figure 9, and nearly half of them should be above $r = 70''$.

The broad distribution of high data points in Figure 9, especially the black band at the very top, shows that most of the outliers cannot be explained by "bad sources" but are consistent with being "bad matches".

The percentage of bad matches is so high because the search circle radius was set to

be $100''$ for all sources, regardless of flux density or calculated position error. In actual practice, nobody blindly identifies an object $100''$ away from a source whose radio position was measured with a beam of FWHM radius $45''/2 = 22\farcs5$. The radius of the circle in which pure position-coincidence identifications are accepted is reasonably chosen to be somewhere between $r_{90} \approx 2.15\,\sigma$ for 90% and $r_{99} \approx 3.03\,\sigma$, and identification candidates at larger separations are rejected. The Appendix of Condon et al. (1975) derives the equations actually used to choose search-circle radii for pure position-coincidence identifications and calculates the resulting identification completeness and reliability. For unresolved NVSS sources, and most NVSS sources are unresolved, these limits are between $\sim 1\farcs1$ and $1\farcs5$ at high flux densities and between $\sim 11''$ and $16''$ at the NVSS sensitivity limit. All candidate matches with larger offsets would be rejected. Figure 9 shows that there are many such points, and counting them as real identifications is responsible for the very high red "empirical" r_{90} line.

A.1.4. The "Resolution" Model for the Matching Radius

The "empirical" model attributing large radio position errors to "bad sources" was used to support the "resolution model" for identifications in Appendix B. The "resolution model" states that the radio-optical matching radius should be fixed at 40% of the FHWM resolution θ for *every* S/N and θ:

"This analysis shows that matching at the $45''$ resolution of NVSS requires a matching radius of $20'' = 40\%$ of the NVSS FWHM resolution. Our experience with the FIRST survey is similar: to get a reasonably complete list of optical identifications we had to use a matching radius of $2'' \sim 40\%$ of the FIRST FWHM resolution. We argue that is a universal requirement for radio sources, at least for sources down to the sub-mJy regime: the matching radius that is required for realistic radio source morphologies is 40% of the FWHM resolution."

This "resolution model" drives All-Sky to higher angular resolution ($\theta \approx 2\farcs5$) than FIRST ($\theta = 5\farcs4$), EMU ($\theta = 10''$), and WODAN ($\theta \approx 16''$):

"WODAN will therefore require an optical matching radius of $6 \times 7''$ and ASKAP-EMU will require $4''$. A cross-match between SDSS and FIRST shows that 34% of FIRST sources have a false (chance) SDSS counterpart within $6\farcs5$. For comparison, 33% of FIRST sources have a true match within $2''$. The conclusion is that half the optical counterparts at SDSS depth will be false matches when using a $6\farcs5$ matching radius.

"The number of false matches can be reduced somewhat by doing a careful analysis of the likelihood of association as a function of separation, but when the starting point is contaminated by 50% of false matches, the final list of identifications will not complete or reliable. The false matching problem will only get worse for deeper optical/IR data."

Appendix B of Murphy et al. (2014b) concludes:

"The bottom line is that we need high resolution to get the accurate positions required for optical identifications. Deeper radio imaging is not a substitute for the necessary resolution. VLASS will be the survey of choice for multi-wavelength science, and an all-sky VLASS will have a long and useful life even after the SKA-precursor surveys are complete."

This conclusion is an essential part of the VLASS justification, so it should be examined very carefully. What if it is wrong, and more sensitive ($\sigma_{\rm n} = 10\,\mu$Jy beam^{-1}) lower-resolution ($\theta = 10''$) surveys like EMU are actually *better* than All-Sky for making complete and reliable optical identifications?

A.2. Position-Coincidence Optical Identifications

There is no doubt that accurate radio positions are needed to make complete and reliable identifications with faint optical objects by position-coincidence alone. A pure position-coincidence identification program chooses the optical object that is both closest to the radio position and lies within a pre-defined search area; if there is no such optical object, there is no identification. The optimum size for the search area is a compromise determined by the combined radio and optical position uncertainties and by the surface density of optical objects. If the chosen search area is too small, the identifications will be very reliable (the reliability R of a set of claimed identifications is the fraction of them that are correct) but incomplete. If it is too large, completeness C is high bu misidentifications are more likely to occur and R is low.

The completeness C of an identification program is the fraction of the radio sources in some complete sample that have identifications brighter than the magnitude limit and that are correctly identified. Higher radio resolution reduces position errors and tends to increase both R and C of sources *in the radio-selected sample*, but the radio sample itself becomes less complete.

The position-coincidence identification completeness C and reliability R of unresolved sources that do make it into the radio catalog are (Condon et al. 1975)

$$C = k^{-1}\left[1 - \exp\left(-\frac{km^2}{2}\right)\right] \tag{A7}$$

and

$$R = C\left\{f^{-1} + (1 - f^{-1})\exp\left[\frac{m^2(1-k)}{2}\right] - \exp\left(-\frac{m^2k}{2}\right)\right\}^{-1}, \tag{A8}$$

where $k \equiv 1 + 2\pi\rho\sigma^2$, ρ is the sky density of identification candidates, $m = r_{\rm c}/\sigma$ is the

cutoff radius of the search circle in units of the rms 1D position error σ, f is the fraction of radio sources having counterparts in the optical catalog, and $(1 - f)$ is the fraction of sources in "empty fields." The free parameter m defining the search area should be small enough for high reliability and large enough for high completeness. A good value for m makes $R \sim C$, and it usually lies in the range $2 \lesssim m \lesssim 3$. If ρ is large, σ must be small to get good completeness and reliability for pure position-coincidence identifications; e.g., $R \sim C \gtrsim 90\%$.

Figure 7 shows $C = R$ for position-coincidence identifications of sources with the faintest optical objects ultimately detectable by the LSST southern sky survey ($r_{\rm AB} < 27.5$, $f \sim 0.9$) and in the HUDF (Beckwith et al. 2006) ($r_{\rm AB} < 29.5$, $f \sim 0.99$) as a function of σ (lower abscissa) and of θ when $S/N = 5$ (upper abscissa). The required radio resolutions for 95% (90%) complete and reliable optical identifications of sources at the survey detection limit $5\sigma_{\rm n}$ are $\theta \leq 4''$ ($6''$) and $\theta \leq 2''$ ($3''$) for the LSST and HUDF, respectively. If the calibration component of EMU position error is $\epsilon < \theta/25 \approx 0\farcs4$ ($\epsilon \sim \theta/90$ for the NVSS), EMU sources stronger than $\sim 13\sigma_{\rm n} \sim 130\,\mu$Jy beam^{-1} can be identified with the faintest LSST objects with 90% completeness and reliability. It appears that the sensitive but low-resolution EMU will be significantly better than All-Sky for completely and reliably identifying radio sources in faint flux-density limited samples with the faintest optical objects in LSST.

A.3. Identifications Using Likelihood Ratios

Optical identifications using only position coincidence ignores prior knowledge about the magnitude distribution of optical identifications. All pure position-coincidence identifications fail when the sky density of optical candidates becomes too high. For example, suppose the entire sky were covered by optical images as sensitive as the HUDF, which contains $\sim 10^3$ objects per square arcmin brighter than $r_{\rm AB} \sim 29.5$ (Beckwith et al. 2006). Would that be a disaster for identifying radio sources in All-Sky or EMU? No, because we already know that most sub-mJy radio sources have counterparts brighter than $r_{\rm AB} \sim 26$ (Ciliegi et al. 2003; Bonzini et al. 2012), so most of their identifications can be recovered by ignoring the countless significantly fainter optical objects. This is effectively what is done when identifications are made with shallower optical images from SDSS, Pan-STARRS, LSST, etc. that can't see the faintest optical objects. The SKADS simulation also predicts that most radio sources stronger than the EMU detection limit will have optical counterparts brighter than $I \sim 25$ (Figure 8). The sky density of such bright galaxies is 50 arcmin^2, so even the very conservative EMU $0.15\,\theta = 1\farcs5$ search radius is good enough for making $> 90\%$ reliable identifications by position-coincidence alone.

Likelihood ratios (Sutherland & Saunders 1992; Ciliegi et al. 2003) formally optimize this Bayesian approach, using prior information about the magnitude distributions, types, colors, etc. of the optical identifications. They often allow identifications to be made even when the position errors are so large that Equations A7 and A8 predict mediocre completeness and reliability. For example, Sutherland & Saunders (1992) developed the mathematics of likelihood ratios to identify galaxies with *IRAS* sources, which have extremely large position errors. Likelihood ratios will certainly be used to supplement position coincidence when identifying weak radio sources in the new surveys with faint optical objects. They will relax the position accuracy requirements and favor lower-resolution surveys that can generate more nearly complete flux-limited samples over high-resolution surveys that cannot. No proposal for high-resolution but incomplete surveys like All-Sky can credibly claim to yield better optical identifications than more complete lower-resolution surveys like EMU without a thorough discussion of likelihood ratios.

A.4. An Empirical Test of the "Empirical" Position Errors

The "empirical" 90%-confidence position errors discussed in Appendix A.1.3 are plotted as a red line in Figure 9. They are much larger than predicted by the "two-component" model (Appendix A.1.2). Figure 9 shows FIRST-NVSS radio position separations for only those FIRST source components that lie within $0\farcs7$ of SDSS optical identifications, so these FIRST positions are accurate proxies for the positions of the optical identifications.

Appendix A.1.3 suggested two explanations for this discrepancy: "bad sources" and "bad matches." In the "empirical" model, there are many "bad sources" whose flux-weighted radio centroids are quite far from their optical identifications (host galaxy or quasar). For bad sources, the "resolution model" (Appendix A.1.4) states that the identification search-circle radius needs to be a large fraction of the FWHM resolution ($0.4\,\theta$), so only high-resolution surveys can make reliable identifications with faint optical objects, regardless of (S/N). The "bad matches" model argues that most of the large FIRST-NVSS separations shown in Figure 9 are caused by FIRST misidentifications of NVSS sources. One reason for bad matches is that there are more FIRST sources per square degree (~ 90) than NVSS sources (~ 53) because FIRST is more sensitive than the NVSS to point sources, so not all FIRST sources actually have real NVSS matches. Appendix B originally included all FIRST-NVSS coincidences having separations up to 100 arcsec, but some of these are just random NVSS sources near faint FIRST sources.

Rick White recently redid the FIRST identifications of NVSS sources by excluding FIRST sources fainter than the NVSS sensitivity limit. Figure 10 is his revised version of

Figure 9. A number of "bad matches" have been eliminated, so the new 90% confidence "empirical" limit shown by the red line is now $\approx 0.15\,\theta \approx 7''$ rather than $\approx 0.4\,\theta$. However, the red line is still much higher than the "two-component" model prediction for high (S/N).

To best way to distinguish between "bad sources" and "bad matches" is to inspect the individual source images. Rick produced a list of 200 FIRST matches with NVSS sources in the narrow NVSS integrated flux-density range $100 \leq S$ (mJy) ≈ 104. The table below shows the first ten and the last 30 sources ordered by increasing FIRST-NVSS separation.

Fri Aug 29 14:02:18 2014
NVSS-FIRST matches with FIRST-SDSS sep < 0.7" sorted by increasing separation
200 sources with NVSS flux density ∼ 100

				-----FIRST--			---NVSS----		--SDSS-	
No.	RA	Dec	Fpeak	Fint	Sep	Fint	Sep	i	Cl
001	16 56 05.204	+15 15 14.00	99.52	103.38	0.07	101.11	0.21	20.31	s
002	10 50 03.740	+51 08 24.13	100.56	104.23	0.08	101.83	0.13	21.01	g
003	16 20 00.478	+40 43 19.04	103.11	103.93	0.11	101.24	0.25	22.39	s
004	11 48 40.790	+54 06 37.22	86.25	88.24	0.14	101.28	0.26	21.77	s
005	09 41 52.435	+27 22 17.84	84.39	85.99	0.14	101.79	0.21	20.07	s
006	09 04 44.337	+23 33 54.05	105.35	107.31	0.17	103.94	0.04	17.00	s
007	22 03 00.068	+02 16 46.04	95.10	102.61	0.17	101.14	0.20	21.81	s
008	14 54 41.019	+20 40 03.17	104.54	109.30	0.19	101.87	0.03	17.58	g
009	16 20 33.436	+17 39 55.46	104.23	111.44	0.19	103.87	0.08	16.41	g
010	12 45 58.839	+54 35 15.85	101.58	104.42	0.19	103.78	0.30	20.28	g
.....									
171	16 20 56.294	+27 34 02.67	2.56	10.75	2.66	100.74	0.11	20.37	s
172	11 03 21.859	+20 48 35.76	60.56	81.34	3.08	100.63	0.49	20.87	g
173	22 42 06.671	+07 31 48.31	7.46	4.19	3.12	103.87	0.10	17.56	g
174	10 03 59.946	+22 52 45.36	55.41	57.74	3.14	101.12	0.22	21.22	s
175	16 35 28.177	+49 08 15.95	24.92	26.76	3.15	100.94	0.24	16.28	g
176	21 19 05.336	-08 11 43.15	96.03	98.30	3.37	103.69	0.25	18.12	s
177	13 41 15.291	+28 16 05.18	87.12	88.26	3.43	100.74	0.17	20.02	s
178	02 50 48.692	+00 02 07.93	11.54	19.17	3.76	100.24	0.60	18.88	s
179	11 52 32.881	+49 39 38.83	41.11	47.08	4.24	101.02	0.18	16.97	s
180	02 53 56.006	-01 13 45.19	26.33	27.00	7.52	100.69	0.40	21.65	s
181	14 05 28.404	+20 50 16.59	16.83	18.57	8.64	103.49	0.16	19.25	g
182	23 11 36.939	-02 09 07.36	29.34	33.31	9.60	103.82	0.05	21.40	g
183	08 32 00.174	+19 53 12.33	59.80	64.31	10.14	101.16	0.29	18.24	s
184	17 09 06.105	+42 01 57.49	5.61	5.67	13.20	103.17	0.19	18.26	g
185	12 01 25.725	+55 32 20.27	6.37	6.07	13.28	101.73	0.29	22.01	g
186	16 49 52.366	+31 08 07.20	21.19	25.84	13.50	100.16	0.41	21.50	g
187	11 05 18.032	+30 09 15.61	2.83	15.05	16.10	101.51	0.26	21.48	g
188	15 53 11.942	+27 33 20.28	10.92	10.30	17.01	103.76	0.40	15.27	g
189	09 02 35.299	-00 21 12.77	6.79	7.48	17.84	102.79	0.30	20.52	g
190	10 36 41.440	+12 33 32.82	2.54	2.20	18.68	103.76	0.02	20.23	g

```
191 07 38 27.603 +24 15 23.36  17.46  58.34 19.48 100.88 0.51 16.49 g
192 13 44 36.420 +16 07 27.86   8.86  10.64 19.96 101.93 0.12 20.61 g
193 13 11 04.669 +27 28 07.46   2.25   3.13 20.57 103.43 0.22 16.99 g
194 14 14 08.431 +48 41 56.23   8.16   7.06 22.18 103.61 0.22 17.84 g
195 14 05 00.812 +29 25 14.03   7.12   7.24 24.68 102.55 0.03 19.77 s
196 16 44 52.560 +37 30 09.26   3.56   3.08 25.05 101.68 0.18 18.07 s
197 08 17 16.145 +07 08 46.49   9.53  10.87 27.63 101.65 0.23 18.15 g
198 10 23 13.604 +63 57 09.23  21.25  21.39 29.39 103.74 0.06 16.95 s
199 12 03 23.678 +13 20 06.77   2.75   3.70 56.56 102.49 0.65 19.15 g
200 11 51 27.937 +36 12 32.20   6.05   5.49 58.39 102.31 0.16 16.73 g
```

The position errors of $S \gg 24$ mJy NVSS sources are completely dominated by calibration errors so the "two-component" model (Equation A6) predicts $\sigma = \sigma_{1D} \approx 0\farcs5$ for unresolved NVSS sources with $S \sim 100$ mJy. The FIRST position errors of such strong sources are much smaller and can be ignored to first order. If the NVSS position error distribution is roughly Gaussian and the sources are "good" (the radio centroid is close to the optical identification), the FIRST-NVSS separations should have a Rayleigh distribution. About 100 of the 200 matches sources should have FIRST-NVSS separations less than $r_{50} \approx 1.18\sigma \approx 0\farcs6$ (Equation A5), and 94 actually do. Likewise, the 180 smallest separations among the the 200 matches should have FIRST-NVSS separations just a little over $r_{90} \approx 2.15\sigma \approx 1\farcs1$, but source number 180 actually has FIRST-NVSS separation $7\farcs52$, putting it close to the red line in Figure 10, and the 200th source has a FIRST-NVSS separation of $58''$. Thus the discrepancy between the "empirical" separations and the separations predicted by the "two-component" model is confined to the large-separation tail of the separation distribution. Are these "bad sources" or "bad identifications"? One clue is their FIRST flux densities, which should be fairly close to the NVSS flux densities, $S \approx 100$ mJy. Most of the 200 FIRST flux densities are indeed close to 100 mJy, but sources 181 through 200 (the 10% with the largest separations) have much lower integrated FIRST flux densities, and ten of them are are below 10 mJy. The 20 sources with the largest separations are worth investigating individually.

Source number 200 has the biggest FIRST-NVSS separation ($58''$). Its NVSS contour plot and FIRST image cutout centered on the optically identified FIRST source are shown in Figure 11. This source is instructive at two levels:
(1) It is a "bad match" in that the optically identified 6 mJy FIRST source is not related to the $S \approx 100$ mJy NVSS source, which is a completely unrelated radio source that happens to lie about 58 arcsec away on the sky. The 113 mJy NVSS source at 11 51 31.66 +36 13 09.5 is closely matched to the strong (also 113 mJy total flux density) FIRST double whose

centroid is at 11 51 31.71 +36 13 09.0, for a true FIRST-NVSS separation of only 0.″8. This source should be moved from the "tail" of large separations, and moving just this one source to 0.″8 separation means that the 90% confidence "empirical" red line should be lowered from the 7.″52 separation of source 180 to the FIRST-NVSS separation of source number 179, 4.″24. Clearly the red lines in Figures 9 and 10 can be sensitive to small numbers of bad matches.
(2) The NVSS and FIRST catalogs do not actually list "radio sources," defined as the total radio emission from a single galaxy or quasar. They only list "radio components," defined as radio image peaks defined by Gaussian fits. The two lobes of the double radio source were not resolved by the NVSS so it is cataloged as a single NVSS component, but the lobes were resolved by FIRST and are cataloged as two FIRST components. The double radio source might also have a "core" component centered on its host galaxy or quasar, but the core is too weak to appear in the FIRST catalog. To make an optical identification of this source, the FIRST components would have be be associated with each other as being the lobes of a single radio source and their centroid position measured. This is an example of using prior knowledge and likelihood ratios instead of just pure position coincidence to make optical identifications. We know that a double source is more likely than two strong, nearly equal sources being so close together, so the identification is likely to lie between the two radio components. The separation of the two lobes is about 14″. If the centroid is typically displaced from the identification by $\sim 10\%$ of the lobe separation (Fomalont 1969), the 1.″4 radio-optical offset is larger than the centroid position error of the NVSS, and having the higher resolution FIRST image would not significantly lower the search-circle radius.

A different kind of "bad match" is illustrated by the 3 mJy FIRST component at 16 44 52.560 +37 30 09.26 (number 196 in the table). It is the core of a triple radio source (Figure 12), and its optical identification with a $g = 18.1$ SDSS quasar at 16 44 52.57 +37 30 09.2 is secure. The NVSS does not detect the core, only the two lobes of this 188 mJy radio source. The bad FIRST-NVSS match is with the northwest radio lobe 25 arcsec away in position angle $-44°$, not with the flux-weighted centroid. The centroid of the NVSS double source is at 16 44 52.83 +37 30 09.5, 3.″2 from the SDSS quasar. This offset is only 5% of the 66 arcsec lobe separation and quite sufficient to make the identification. Thus this is not a "bad source," but the ability of FIRST to detect the core separately is still an advantage, leading to a subarcsec radio-optical offset, while the NVSS radio-optical offset is 3.2 arcsec. On the other hand, the core flux density is only 3× the FIRST detection limit, so if this source were $4X$ less luminous or twice as far away, FIRST would not detect the core. Then FIRST would be at a disadvantage because it misses about 50 mJy of the lobe flux, so the FIRST centroid position at 16 44 52.44 +37 30 14.5 is less accurate, being 5.″2 from the optical position.

Which of the final 20 sources in the list are bad matches with completely unrelated stronger sources? The 3.7 mJy FIRST source number 199 at 12 02 23.678 +13 20 06.77 has the second-largest FIRST-NVSS separation (56″). The correct match for the unresolved 103 mJy NVSS source at 12 03 20.68 +13 19 30.9 is the single-component 105 mJy FIRST source at 12 03 20.649 +13 19 31.45, and their FIRST-NVSS separation is 0.″6. This association is confirmed by the optical identification of the NVSS source with the galaxy 2MASX J12032061+1319316, also 0.″6 from the NVSS position. The 3 mJy FIRST source number 192 at 13 44 36.420 +16 07 27.86 is unrelated to the much stronger NVSS/FIRST source at 13 44 36.06 +16 07 08.7. The strong source has a flat radio spectrum, so it unlikely to be a lobe of source 192. The 2.2 mJy FIRST source number 190 at 10 36 41.440 +12 33 32.82 is unrelated to the ∼ 100 mJy NVSS/FIRST source which is identified with a 2MASS $z = 2.145$ quasar at 10 36 40.36 +12 33 38.9. The 7 mJy FIRST source number 189 at 09 02 35.299 −00 21 12.77 appears to be unrelated to the stronger NVSS/FIRST double source to the east. The weak, extended FIRST source number 187 is in the lobe of the unrelated triple source identified with a bright galaxy whose core is at 11 05 22.861 +30 09 41.46. Removing these bad matches from the list lowers the 90% FIRST-NVSS separation to ≈ 3.″2, or ≈ $0.07\,\theta$.

Most of the remaining sources in the "top 20" are bad matches with individual NVSS lobes of double sources larger than ∼ 60″ rather than with the NVSS centroids. Many of these NVSS centroids may be farther than 3.″2 to the radio cores, so they won't lower the estimated 90% separation by much. Replacing the component offsets with centroid offsets will, however, greatly shorten the long "tail" of large offsets and eliminate the conspicuously high points in Figures 9 and 10.

Further refining the Appendix B approach to calculating the resolution θ required to make deep optical identifications is probably not worthwhile because:
(1) The sample is biased by the high resolution of FIRST, so it excludes many extended sources, spiral galaxies in particular.
(2) The optical identifications were made with cataloged FIRST source components, not with complete radio sources. Thus triple sources with sufficiently strong cores have been identified, but most double sources have not.

I conclude that 90% of the identifications conservatively lie within $0.1\,\theta$; a $0.4\,\theta$ search radius is unnecessarily large. The "resolution" model in Appendix B of Murphy et al. (2014b) indicated that a VLASS with $\theta = 3''$ resolution and a $0.4\,\theta = 1.''2$ identification search radius can make reliable deep position-coincidence identifications while EMU with $\theta = 10''$ and a 4″ search radius cannot. However, a 1.″2 search radius is $0.12\,\theta$ for EMU, which easily satisfies the conservative new $0.1\,\theta$ requirement, so the high resolution of All-Sky is not needed for

identification reliability and will hurt identification completeness. EMU is far more sensitive than All-Sky to both unresolved cores and extended emission from lobes and spiral galaxies, making it better than All-Sky for complete as well as reliable optical identifications.

REFERENCES

Aaquist, O. B., & Kwok, S. 1990, A&AS, 84, 229

Becker, R. H., White, R. L., & Helfand, D. J. 1995, ApJ, 450, 559

Beckwith, S. V. W. et al. 2006, AJ, 132, 1729

Bevington, P. R. 1969, "Data Reduction and Error Analysis for the Physical Sciences," (McGraw-Hill, New York)

Bondi, M., Ciliegi, P., Schinnerer, E., Smolcic, V., Jahnke, K., Carilli, C., & Zamorani, G. 2008, ApJ, 628, 1129

Bonzini, M., Mainieri, V., Padovani, P., Kellermann, K. I., Miller, N., Rosati, P., Tozzi, P., Vattakunnel, S., Balestra, I., Brandt, W. N., Luo, B, & Xue, Y. Q. 2012, ApJS, 203:15

Bridle, A. H., Backer, D. C., Churchwell, E. B., Haynes, M. P., Hewitt, J. N., Hogg, D. E., & Lo, K. Y. 1997, "Report of the NRAO Large Proposal Committee", posted as an attachment on
`https://staff.nrao.edu/wiki/bin/view/NM/VLASSSciStaffForum`

Chang, T. C., Refrigier, A., & Helfand, D. J. 2004, ApJ, 617, 794

Ciliegi, P., Zamorani, G., Hasinger, G., Lehmann, I., Szokoly, G., & Wilson, G. 2003, A&A, 398, 901

Condon, J. J. 1984, ApJ, 287, 461

Condon, J. J. 1989, ApJ, 338, 13

Condon, J. J. 1997, PASP, 109, 166

Condon, J. J. 2014, "VLASS Notes, 2014 September 23", posted as an attachment on
`https://staff.nrao.edu/wiki/bin/view/NM/VLASSSciStaffForum`

Condon, J. J., Balonek, T. J., & Jauncey, D. L. 1975, AJ, 80, 887

Condon, J. J., Cotton, W. D., & Broderick, J. J. 2002, AJ, 124, 675

Condon, J. .J., Cotton, W. D., Greisen, E. W. et al. 1998, AJ, 115, 1693

Condon, J. J., Kellermann, K. I., Kimball, A. E., Ivezic, Z., & Perley, R. A. 2013, ApJ, 768:37

Condon, J. J., & Kaplan, D. L. 1998, ApJS, 117, 361

Fomalont, E. B. 1969, ApJ, 157, 1027

Hodge, J. A., Becker, R. H., White, R. L., Richards, G. T., & Zeimann, G. R. 2011, A. J., 142:3

Hummel, E. 1981, A&A, 93, 93

Lindsay, S. N., Jarvis, M. J., Santos, M. G., Brown, M. J. I., Croom, S. M., Driver, S. P., Hopkins, A. M., Liske, J., Loveday, J., Norberg, P., & Roboham, A. S. G. 2014, MNRAS, 440, 1527

Magliocchetti, M., et al. 2002, MNRAS, 333, 100

Murphy, E., Baum, S., et al. 2014, "VLASS Project Description" (August 1 version)

Murphy, E., Baum, S., et al. 2014, "The Jansky-Very Large Array Sky Survey (VLASS)" (August 8 version)

Norris, R. P. et al. 2011, PASA, 28, 215

Ray, P. S. et al. 2012, arXiv:1205.3089

SSG15, VLA Survey Science Group 2015, VLASS "final" proposal
`https://safe.nrao.edu/wiki/pub/JVLA/VLASS/VLASS_final.pdf`

Sutherland, W., & Sanders, W. 1992, MNRAS, 259, 413

White, R. L., Becker, R. H., Helfand, D. J., & Gregg, M. D. 1997, ApJ, 475, 479

Wilman, R. J., Miller, L., Jarvis, M. J. et al. 2008, MNRAS, 388, 1335

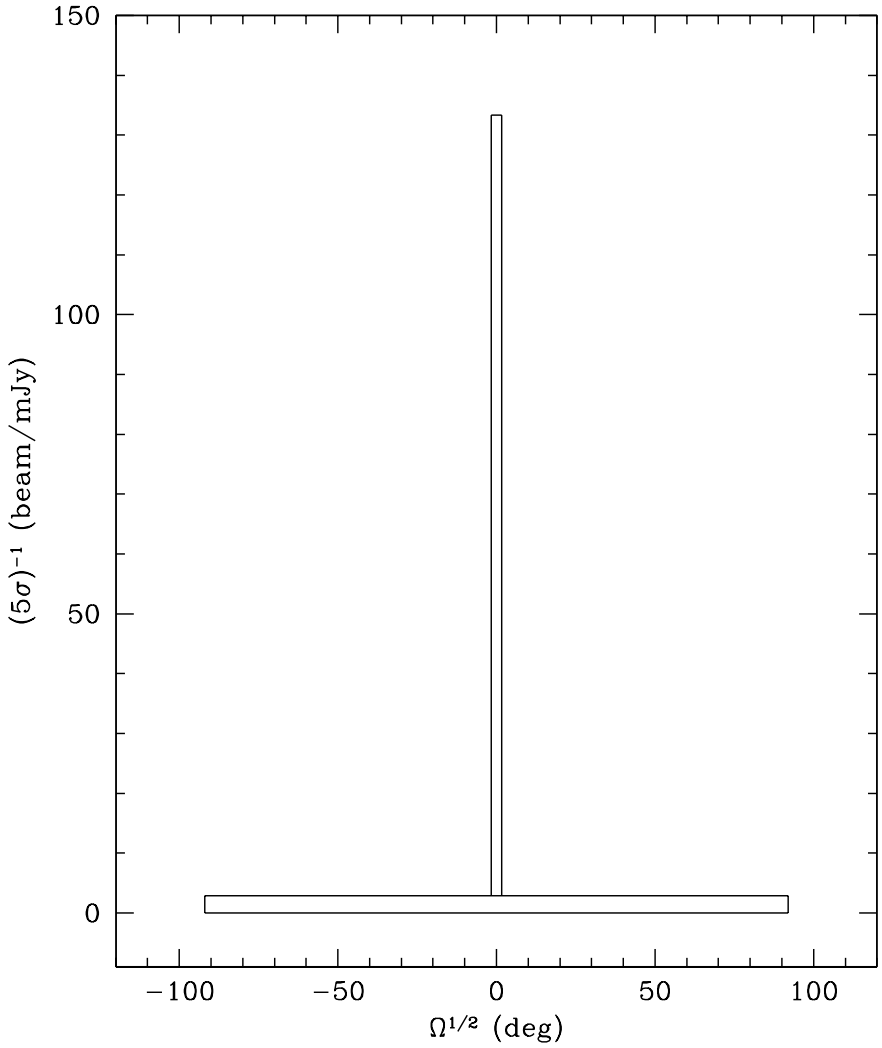

Fig. 1.— The VLASS is more like a Prussian hat than a traditional wedding cake. The layers are All-Sky (bottom) and Deep (top). The plotted width of each layer is $\Omega^{1/2}$, appropriate for a square cake. The height of each layer is proportional to the point-source detection sensitivity. Abscissa: $\Omega^{1/2}$ (deg) Ordinate: Point-source $(5\sigma)^{-1}$ sensitivity (beam mJy^{-1})

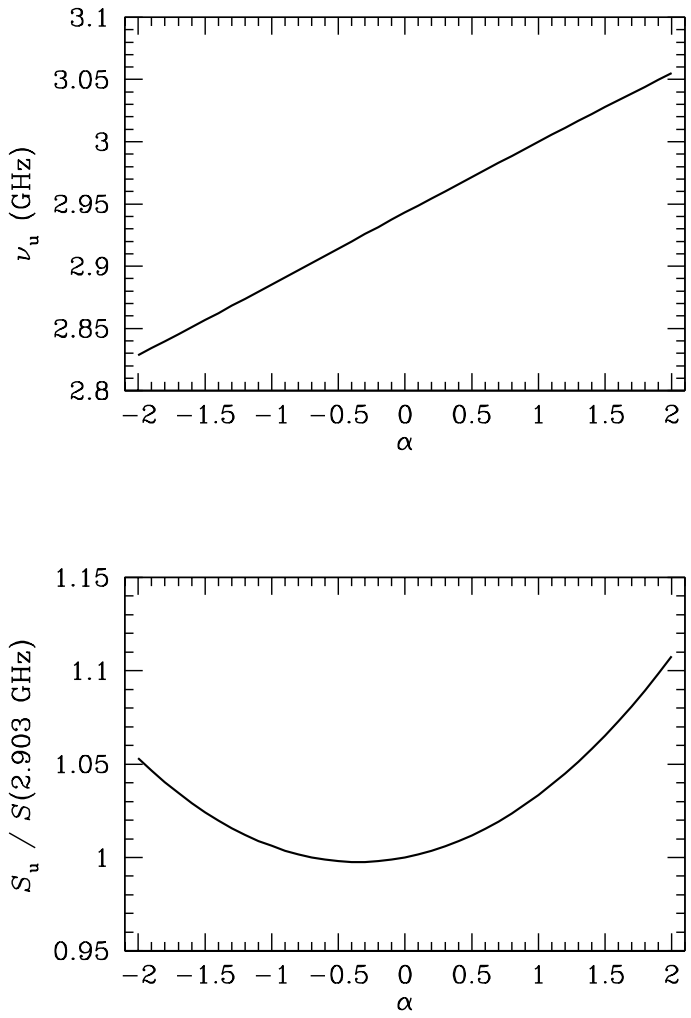

Fig. 2.— The top panel shows the frequency $\nu_{\rm u}$ at which the spectrally unweighted VLA S-band ($2 \leq \nu\,({\rm GHz}) \leq 4$) image flux density is correct, as a function of source spectral index α. For sources with typical spectral index $\alpha = -0.7$, $\nu_{\rm u} \approx 2.903$ GHz. If $\nu_{\rm u} = 2.903$ GHz is taken to be the nominal image frequency, the ratio of the source flux density $S_{\rm u}$ near the center of the broadband image will differ from its true $S(2.903\ {\rm GHz})$ flux density by the flux-density ratio plotted as a function of source spectral index in the bottom panel. $S_{\rm u}$ is within 1% of $S(2.903\ {\rm GHz})$ over the spectral range $-1.2 < \alpha < +0.5$ that includes nearly all sources in samples complete at frequencies near $\nu \sim 3$ GHz.

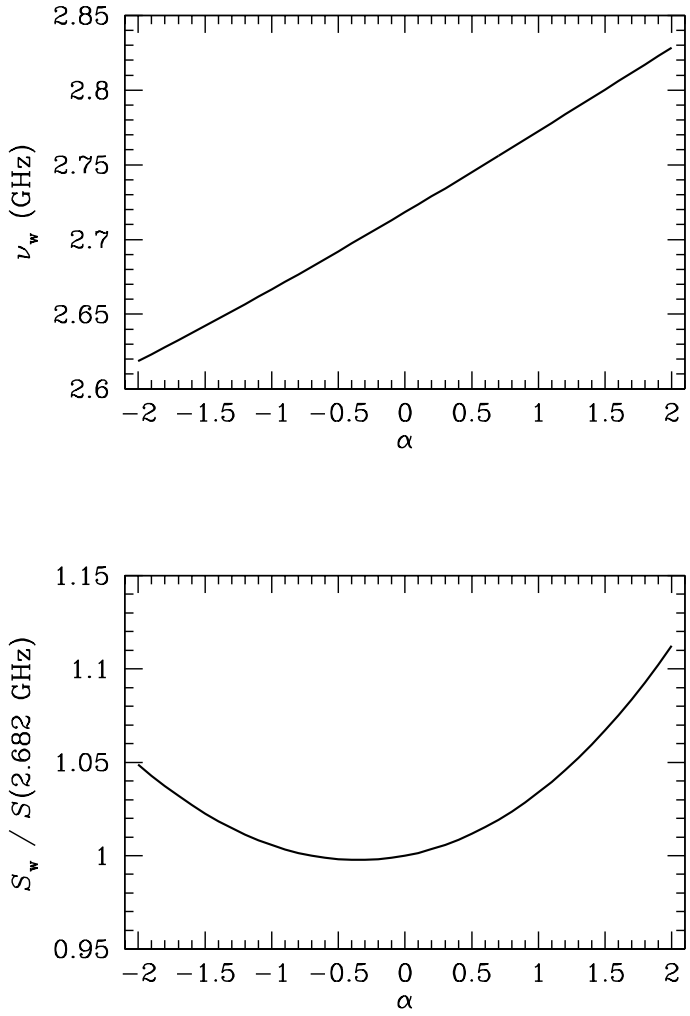

Fig. 3.— The top panel shows the frequency $\nu_{\rm w}$ at which the spectrally weighted VLASS image flux density is correct, as a function of source spectral index α. For sources with typical spectral index $\alpha = -0.7$, $\nu_{\rm w} \approx 2.682$ GHz. If $\nu_{\rm w} = 2.682$ GHz is taken to be the nominal VLASS image frequency, the ratio of the source flux density $S_{\rm w}$ in the broadband survey image to its true $S(2.682$ GHz) flux density is plotted as a function of source spectral index in the bottom panel. $S_{\rm w}$ is within 1% of $S(2.682$ GHz) over the spectral range $-1.2 < \alpha < +0.5$ that includes nearly all sources in samples complete near frequencies $\nu \sim 3$ GHz.

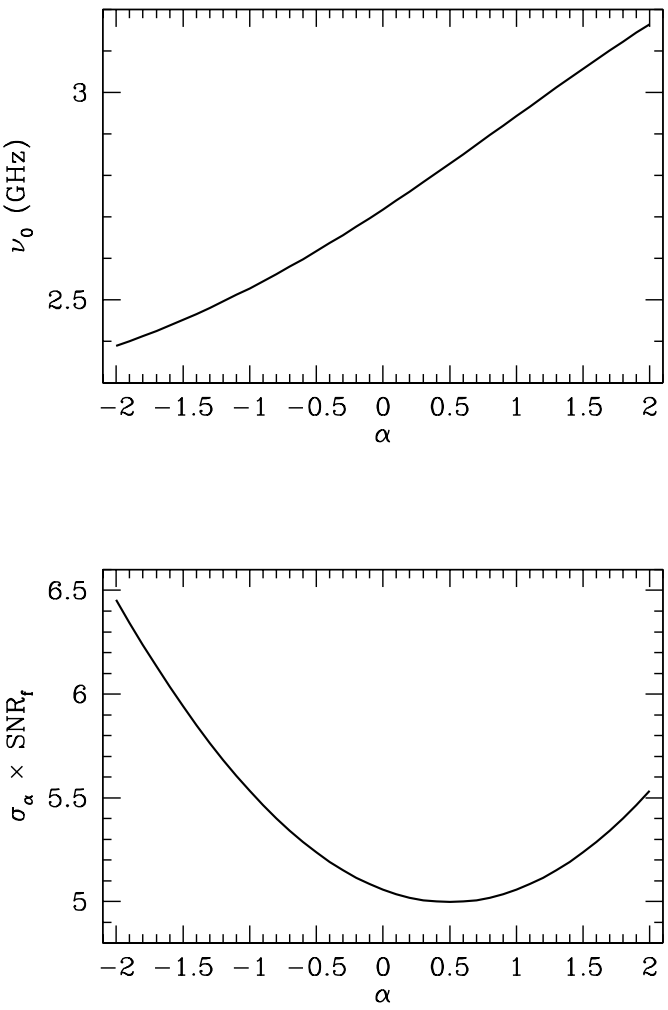

Fig. 4.— The top panel shows the fitting "pivot" frequency $\nu_0 = \bar{\nu}_\mathrm{h}$ (Equation 44) as a function of source spectral index α for the VLASS survey in which the integration time $\tau \propto \nu^{-2}$. The bottom panel shows the product of the rms uncertainty σ_α in the spectral index α and the signal-to-noise ratio $\mathrm{SNR_f}$ of the fitted flux density at frequency $\nu_0 = \bar{\nu}_\mathrm{h}$ as a function of source spectral index α for the VLASS. The same curves apply to S-band pointed observations of sources much smaller than the primary beam if the values of α on the abscissae are reduced by exactly 1.0; e.g., a survey $\alpha = 0$ corresponds to a pointed $\alpha = -1.0$.

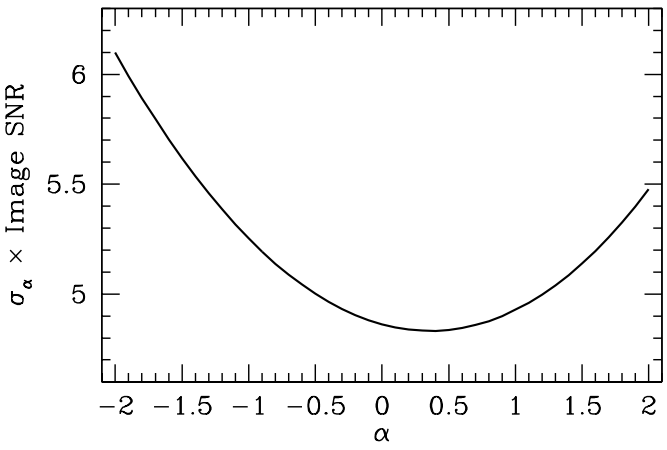

Fig. 5.— The product of the rms uncertainty σ_α in the spectral index α and the signal-to-noise ratio on a VLASS image (Image SNR) is plotted as a function of source spectral index α.

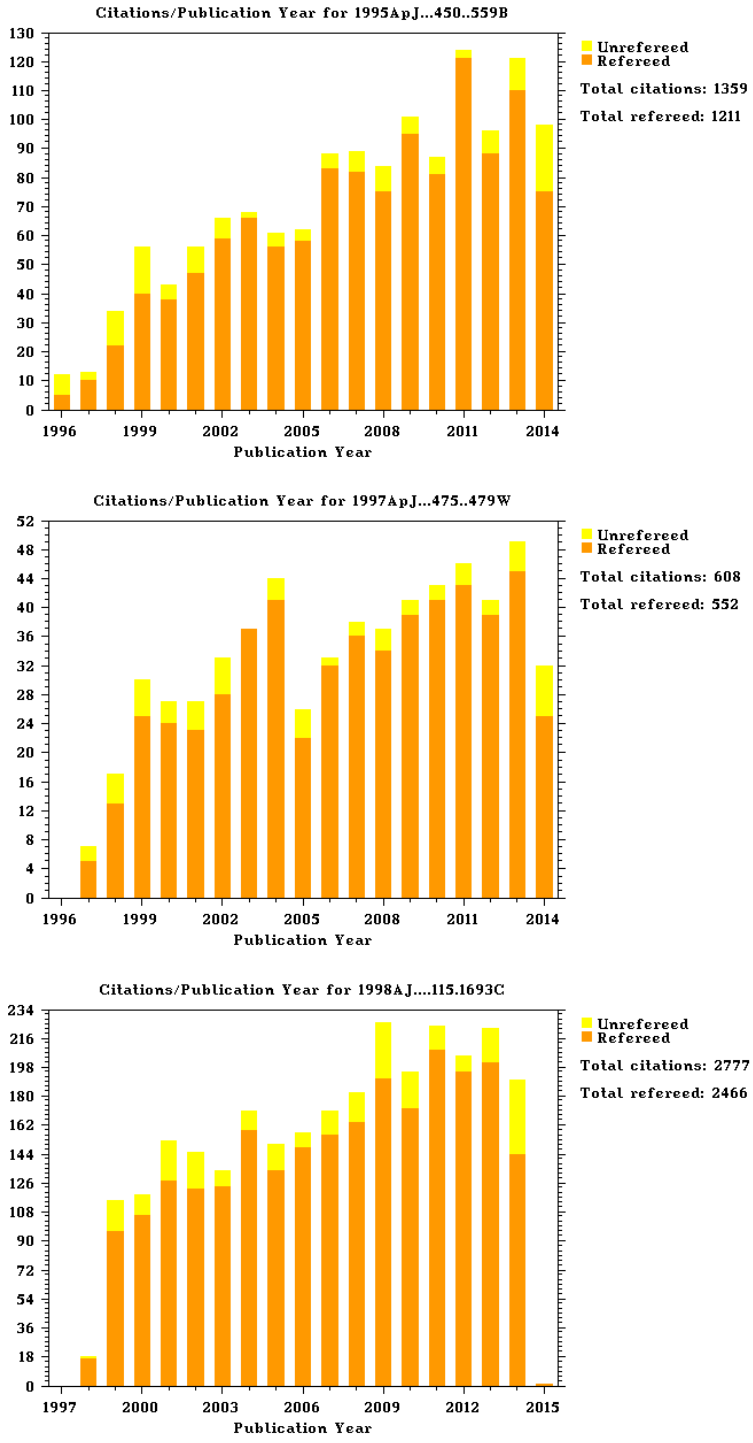

Fig. 6.— Citation histories for the FIRST survey images (Becker et al. 1995), the FIRST survey catalog (White et al. 1997), and the NVSS (Condon et al. 1998) as of 2014 September 23.

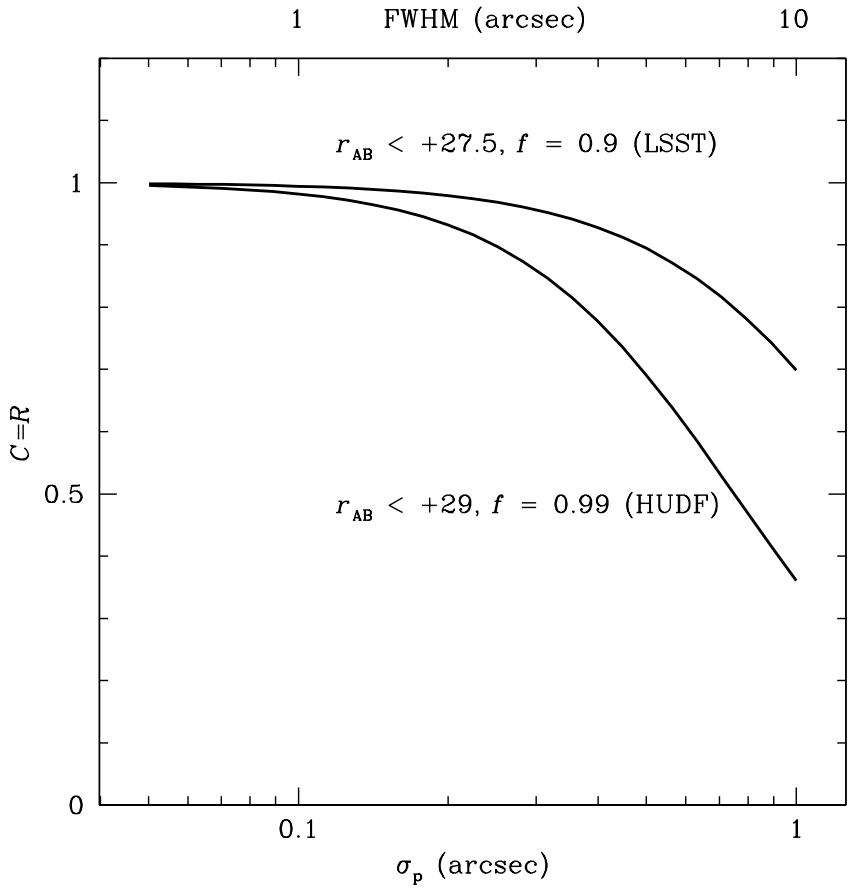

Fig. 7.— If the search-circle radius is chosen such that identification completeness C and reliability R are about equal, the rms position error $\sigma_{\rm p}$ is determined by the sky density of optical identification candidates and the fraction f of radio sources having optical counterparts. The two curves show the values of $C = R$ for "blind" position-coincidence identifications to the limits of the planned LSST survey and the HUDF. Lower abscissa: rms position error in each coordinate (arcsec). Upper abscissa: maximum PSF FWHM (arcsec) for which the noise error on an $SNR = 5$ source equals $\sigma_{\rm p}$. Ordinate: Completeness and reliability.

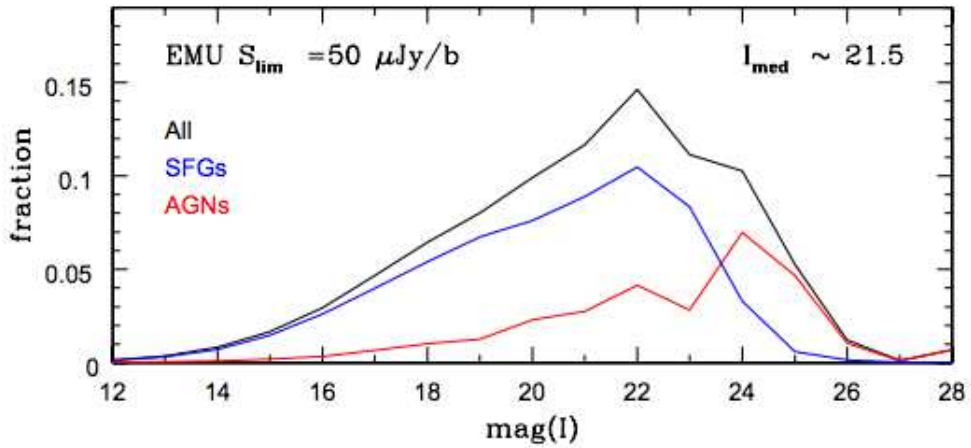

Fig. 8.— The I-band magnitude distributions from the SKADS simulation for all radio sources stronger than 50 μJy beam^{-1} (black), star-forming galaxies (blue), and AGNs (red). Nearly all of the optical counterparts are brighter than $I \sim 25$, well above the LSST limit shown in Figure 7.

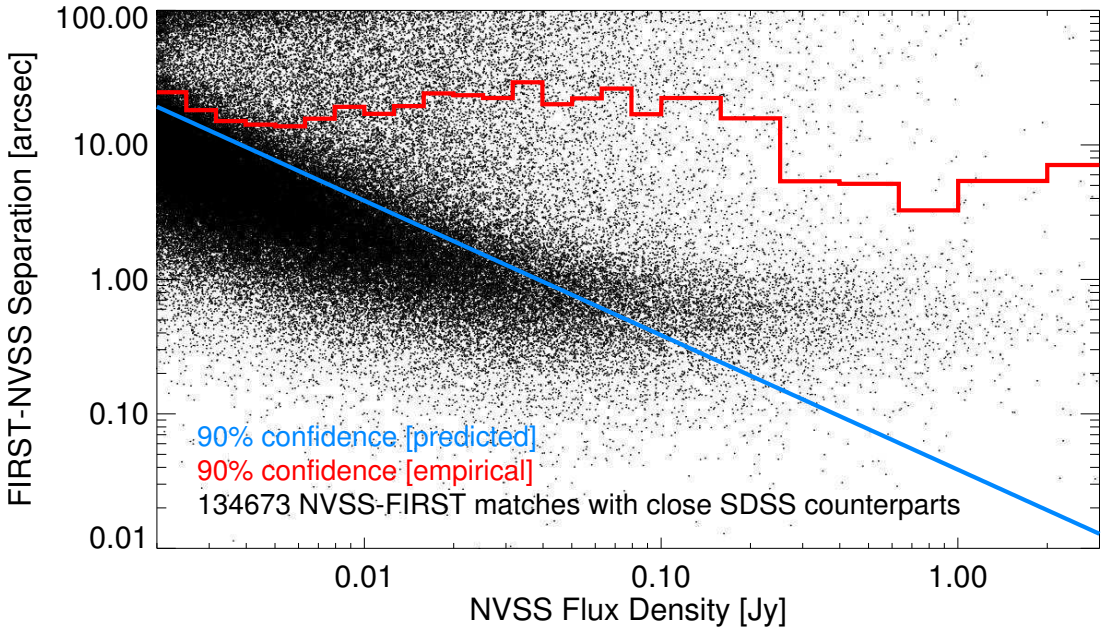

Fig. 9.— This is the original version of the FIRST-NVSS separation plot in Appendix B of Murphy et al. (2014b). The red line shows the 90% confidence "empirical" separation as a function of NVSS flux density. It suggests that the identification search radius needs to be about 0.4 times the NVSS FWHM resolution $\theta = 45''$ even at fairly high flux densities $S \sim 100$ mJy.

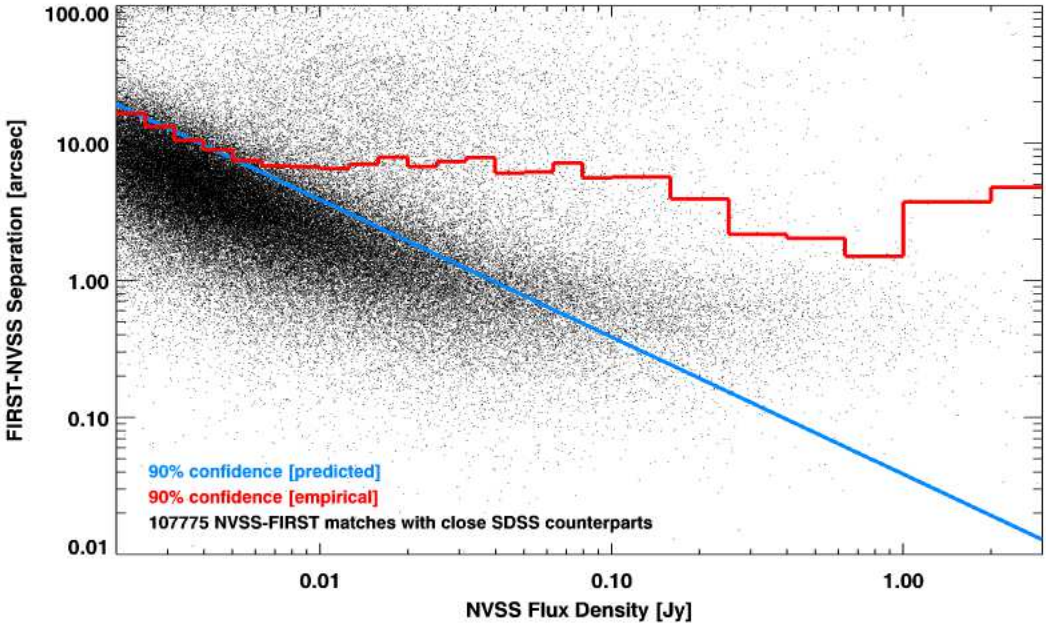

Fig. 10.— Rick White's revised version of the FIRST-NVSS separation plot. The red line is lower and corresponds to about 0.15 times the NVSS FWHM resolution at high flux densities, but it is still higher than expected from the "two component" model for identifying compact or symmetric sources.

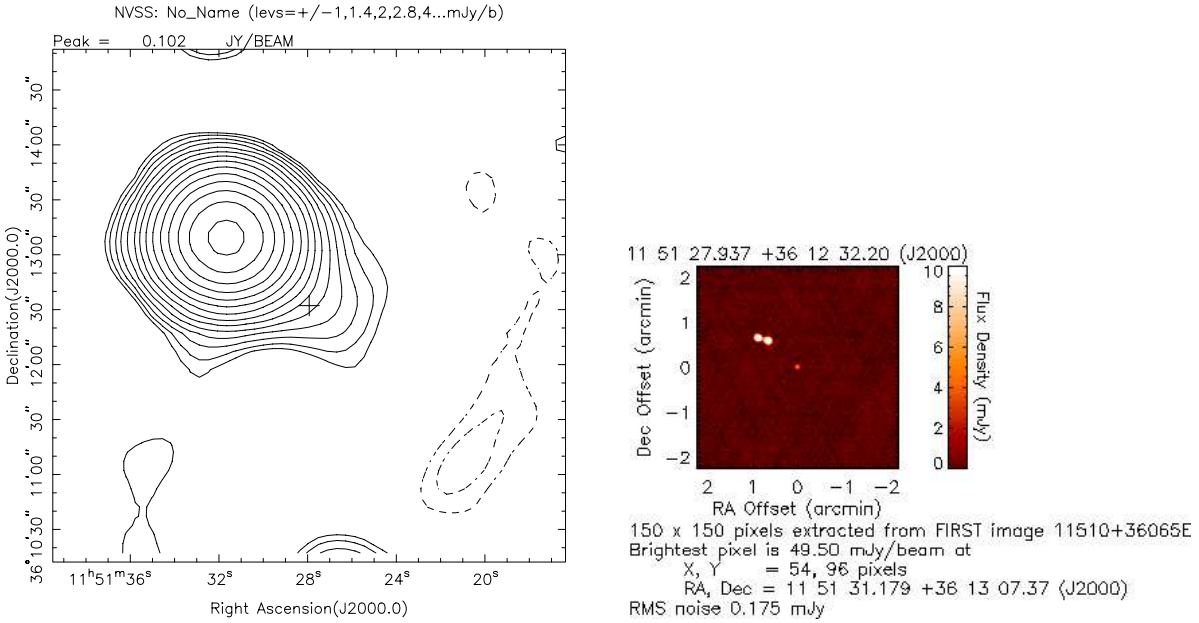

Fig. 11.— This NVSS contour plot and FIRST cutout are both 4.5 arcmin on a side and centered on FIRST 115127.94+361232.2, a 6 mJy FIRST point source identified with an SDSS galaxy. This faint FIRST source at the position of the cross is visible only as a tail extending from the main NVSS source. The correct NVSS source match is the 113 mJy FIRST double source to the northeast, which is a background source unrelated to the FIRST point source.

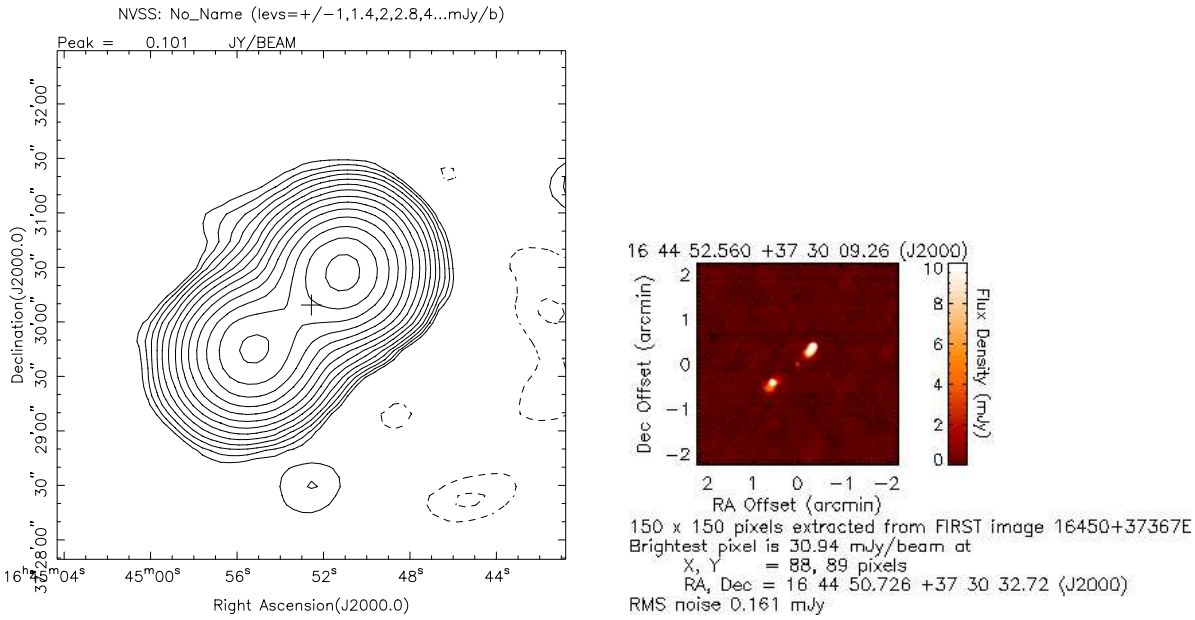

Fig. 12.— This NVSS contour plot and FIRST cutout are both 4.5 arcmin on a side and centered on FIRST 164452.56+373009.3, a 3 mJy FIRST point source correctly identified with an SDSS galaxy. It is the core of a triple source whose total FIRST flux density is 137 mJy. It was matched with the northeast component only of the 188 mJy NVSS double, so it is another "bad match".